Stockholm University

Sensitivity studies of models of voltage-dependent conductance in neurons

Tom Andersson

Licentiate Thesis in Mathematical Statistics at Stockholm University, Sweden 2010

Mathematical statistics
February 2010
www.math.su.se

Mathematical statistics
Department of Mathematics
Stockholm University
SE-106 91 Stockholm

Sensitivity studies of models of voltage-dependent conductance in neurons

Tom Andersson

February 11, 2010

Licentiate Thesis

Stockholm University Department of Mathematics
Section for Mathematical Statistics toma@math.su.se +46 70 594 43 23

Abstract

This thesis consists of two manuscripts: "Exploring voltage-dependent ion channels *in silico* by hysteretic conductance" by Tom Andersson, and "Statistical sensitivity analysis and remodeling of whole-cell conductances in nociceptors" by Tom Andersson, Joanna Tyrcha and Olivia Eriksson.

The general approach to modeling neuronal excitability is to formalize and simulate systems of ordinary differential equations that describe voltage-dependent and ionic specific conductances of cell membranes. The systems are deterministic in nature, but rely on a large number of uncertain parameter estimations. The uncertainty is usually ignored and left out of account when analyzing neuronal excitability by means of conductance models. Here we present two sensitivity studies of voltage-dependent conductance models demonstrating the value of both systematic and random parameter variations in formalizing and evaluating model components of membrane excitability.

In the first study, we put a specific sensitivity measure to use, i.e. hysteretic conductance (conductance loops), to explore the state space and kinetics of voltage-dependent ion channels. In the second study, we evaluate response effects of parameter variations in a conductance model of nociceptors, revealing critical regulatory parameters by statistical analysis. The studies show that designed sensitivity measures and statistical methods can reveal new conductance mechanisms and regulatory pathways in existing neuronal conductance models.

Key words: whole-cell model, ion channel, Hodgkin-Huxley, Markov model, sensitivity analysis, nociceptor

1 Acknowledgements

This work is supported by the Swedish Foundation for Strategic Research and The Foundation of Helge Ax:son Johnson.

I express my warm gratitude to my supervisors Joanna Tyrcha, Juni Palmgren and Olivia Eriksson for their generous support, encouragement and critical reflections.

2 Introduction

The two basic elements of neuronal conductance models is the capacitance function of the cell membrane and the conductance function of transmembrane proteins [5][8], i.e. proteins interspersed in the cell membrane regulating ion transport across the membrane, e.g. ion pumps and ion channels. The membrane consists of a lipid bilayer, enclosing the cell interior and blocking passive diffusion of ions. It allows charge to be stored on each side of the cell membrane, thereby functioning as a capacitor. Transmembrane proteins regulate ionic transport and contribute to ion specific gradients across the membrane, thereby generating ion specific currents and the membrane potential.

We describe the capacitor function by the following equation:

$$C\,\dot{V}_m = -\sum_{k=1}^{N} I_k + I_{inj} \tag{2.1}$$

where C is the capacitance (Farad F), $\dot{V}_m$ is the time derivative of the membrane potential (V_m per second), and I_k is an ionic current (Ampere A). The sum of all ionic currents $\sum_{k=1}^{N} I_k$ ($k \in \{\mathrm{Na}^+, \mathrm{K}^+, \mathrm{Ca}^{2+}, \mathrm{Cl}^-\}$ make up the whole-cell current, consisting of ion pumps sustaining the membrane resting potential, i.e. ionic transport driven by chemical energy, and ion channels regulating ionic currents driven by ionic gradients. I_{inj} is the external current in an electrophysiological experiment, with reversed sign due to its nature, i.e. an outward electron flow making a positive current, in contrast to an outward ionic flow making a negative current.

Applied to cell membranes, C and I are relative to the surface area and units are often standardized in modeling studies (F and A per unit area). C is usually considered a constant, whereas the ionic currents I_k are the main object of analysis.

$$I_k = G_k(V_m, M)(V_m - E_{ion}) \tag{2.2}$$

The ionic current I_k depends on the ion specific conductance of the cell membrane $G_k(V_m, M)$, where M represents any modulator of the ionic specific conductance. It also depends on the driving potential, i.e. the

membrane potential minus the reversal potential of the ionic current. The reversal potential is usually considered a constant. By allowing for multivariate and non-linear conductance functions $G_k(M, V_m)$, the equations form a system of equations that may generate diverse responses, i.e. resting states and patterns of voltage oscillation.

The voltage-dependent and ionic-specific conductances are critical membrane components in the active regulation of membrane excitability and action potentials (neuronal spikes) [1]. Thus, the challenge in neuronal modeling of membrane excitability is how to identify and define conductance components and functions $G_k(M, V_m)$. Generally speaking, there are two approaches: (1) whole cell records and (2) single channel records [3]. The former is a macroscopic aggregation of microscopic currents through thousands of ion channels, smoothing out the details of specific and single ion channel activity. In contrast, single channel records reveal the gating process of a single protein, i.e. discrete changes in conductance over time. However, the distinction between macroscopic and microscopic conductances is not clear-cut. There are experimental methods mixing the levels, e.g. gene expression of specific ion channels in different quantities in a single cell, allowing for mesoscopic studies of specific ion channels.

Macroscopic and microscopic models of ionic conductance tend to be different. In macroscopic studies, the focus is on the whole-cell membrane potential, for which reason models of specific ionic conductances are kept simple. The main challenge is instead to account for the variety of conductances regulating membrane excitability. The original study of the giant squid axon by Hodgkin and Huxley is an example of this [4]. Voltage-dependent and ionic specific conductance are then assumed to consist of voltage-sensitive "gating particles" that move across the membrane in response to voltage change, thereby changing ionic specific conductances:

$$G_k(M, V_m) = G^{max} p_{open} \tag{2.3}$$

$$p_{open} = \prod_{k=1}^{N} p_k \tag{2.4}$$

$$\dot{p}_k = \alpha(M, V_m) - (\alpha(M, V_m) + \beta(M, V_m))p_k \tag{2.5}$$

$$= \frac{p_k(\infty) - p_k}{\tau} \tag{2.6}$$

where G^{max} is the maximum conductance of an ionic conductance, p_{open} is the active proportion of conductance at a certain moment in time, defined as the product of the open probability p_k of N independent gating particles. The "rate constants" α and β ($\tau = \frac{1}{\alpha+\beta}$) represent the rates of change between active (open) and inactive (closed) states of a single gating particle:

$[C] \underset{\beta}{\overset{\alpha}{\rightleftharpoons}} [O]$. Although called "constants", in reality, they correspond to multivariate rate functions [6], $\alpha(V_m, M)$ and $\beta(V_m, M)$, thereby increasing the complexity of conductance models.

In microscopic single ion channel studies [12], it is clear that the macroscopic modeling approach is a simplification. The state space and kinetics of ion channels are more diverse and plastic than what is assumed in macroscopic models. The Hodgkin-Huxley assumption of independent gating particles is often not met. To account for microscopic conductance properties, we must assume a larger set of ion channel states and pathways. Markov models are then often used to formalize the state space and the transition rules that regulate p_{open}. Some scholars claim that also this approach is insufficient, that we need to use fractal models to fully account for ion channel structure and dynamics [9]. However, here we limit the discussion to traditional Hodgkin-Huxley and Markov models. They are still the main approaches to neuronal conductance modeling, and there is still much to be learned from them [10].

Irrespectively of the level of analysis, the general approach to conductance modeling is to formalize a system of equations in agreement with experimental research, thereafter simulate the model and compare its performance to recorded data. Seldom do studies address the question of the role of experimental protocols and parameter variation for model performance [7][11]. In mathematics and statistics, this line of inquiry is called "sensitivity analysis" [13], i.e. analysis of the relative importance of model parameters to model performance. Here we also stress the need for developing relevant response measures and evaluating parameter distributions when carrying out sensitivity analysis. For this reason, we describe the work underlying this thesis in broader terms, "sensitivity studies", i.e. *studies of model performance in response to parameter variations*, the purpose being to identify and evaluate critical and modulatory parameters in regulating model performance [2].

In the first article, we explore "hysteretic conductance", i.e. conductance loops in response to periodic voltage stimulation, as a response measure of ion channel kinetics, i.e. independent and cooperative gating, as well as mode-shifts, i.e. interactions between voltage-dependent and independent gating mechanisms. We show that it can reveal kinetic properties that may otherwise remain invisible with traditional experimental and simulation protocols. In the second article, we carry out a more complete sensitivity analysis of a neuronal conductance model, including the design of relevant response measures, as well as statistical analysis of parameter variation and mathematical modeling of response effects. Together, the two articles show the value and use of sensitivity studies for the purpose of developing and evaluating neuronal conductance models.

References

[1] Baranauskas, G. Ionic Channel Function in Action Potential Generation: Current Perspective. Molecular Neurobiology (2007) 35:129-150.

[2] Eriksson, O., Andersson, T., Zhou, Y. and Tegnér, J. Decoding complex cellular networks - critical, modulatory and silent parameters. Submitted to BMC Systems Biology.

[3] Hille B. Ion Channels of Excitable Membranes. Sunderland, US: Sinauer Associates Inc, 2001 (3^{rd} edition).

[4] Hodgkin, A.L. and Huxley, A.F. A quantitative description of membrane current and its application to conduction and excitation in nerve. The Journal of Physiology. 1952. 117:500-544.

[5] Izhikevich, E.M. (2007). Dynamical systems in neuroscience: The geometry of excitability and bursting. Cambridge, Massachusetts: MIT Press.

[6] Jones, S.W. Are rate constants constant? The Journal of Physiology. 2006. 571(3):502.

[7] Kargol, A, Smith, B and Millonas, M. Application of nonequilibrium response spectroscopy to the study of channel gating. Experimental design and optimization. Journal of Theoretical Biology. 2002; 218:239-258.

[8] Kock, C. Biophysics of Computation: Information Processing in Single Neurons. New York, US: Oxford University Press. 1999.

[9] Liebovitch, L.S., Scheurle, D., Rusek, M., Zochowski, M. Fractal methods to analyze ion channel kinetics. Methods. 2001. 24:359-375.

[10] McCormick, D.A., Shu, Y., and Yu, Y. Hodgkin and Huxley model - still standing? Nature. 445(4) January 2007.

[11] Millonas, M and Hanck, DA. Nonequilibrium response spectroscopy of voltage-sensitive ion channel gating. Biophysical Journal. 1998;74:210-229.

[12] Sackmann, B. and Neher, E. (Eds.) Single-Channel Recordings. 1995. 2^{nd}Ed. New York, US: Plenmum Press.

[13] Saltelli, A., Chan, K., and Scott, E.M. (Eds.) (2000). Sensitivity Analysis. Chichester, UK: John Wiley & Sons Ltd.

Exploring voltage-dependent ion channels *in silico* by hysteretic conductance

Tom Andersson

February 11, 2010

Stockholm University
Department of Mathematics
Section for Mathematical Statistics toma@math.su.se +46 70 594 43 23

Abstract

Kinetic models of voltage-dependent ion channels are normally inferred from time records of macroscopic current relaxation or microscopic single channel data. A complementary explorative approach is outlined. *Hysteretic conductance* refers to conductance delays in response to voltage changes, delays at either macroscopic or microscopic levels of observation. It enables complementary assessments of model assumptions and gating schemes of voltage-dependent channels, e.g. independent versus cooperative gating, and multiple gating modes. Under the Hodgkin-Huxley condition of independent gating, and under ideal measurement conditions, hysteretic conductance makes it also possible to estimate voltage-dependent rate functions. The argument is mainly theoretical, inspired by experimental observations, and illustrated by simulations of Markov kinetic models.

Key words: voltage-gated ion channels, hysteretic conductance, kinetic Markov models

Contents

1 Introduction

Ion channels are nanoscopic, transmembrane, pore-forming proteins that maintain and regulate ionic currents through the cell membrane. They are the key dynamic elements in maintaining membrane excitability and generating neural signals (action potentials) [6][17]. In large numbers, thousands on a microscopic scale, they either sustain a membrane potential around -60mV/-80mV (zero outside, negative inside), or generate action potentials about 80-100mV in amplitude. This dynamic function depends on the capacity of voltage-dependent ion channels to change the permeability of ions in response to voltage change across the cell membrane. At the level of a single channel, the gating process involves conformational changes of the protein, resulting in alternations between open and closed states. Due to energy fluctuations, the transitions are random in nature.

With increasing precision, electrochemical and pharmacological studies, in combination with bioengineering and computational science, can record ionic conductances in whole cells or at the level of single channels. There is an ongoing proliferation of measurement techniques and methods of analysis [7][15][24][26][35][37][38][43][44]. For modeling purposes, however, we can classify a major part of the data into two categories, (1) whole cell records of relaxation and (2) single channel records of dwell time. The former is a macroscopic aggregation of microscopic currents through thousands of ion channels, smoothing out the details of single channel activity. It was used by Hodgkin and Huxley (HH) in their classic study of action potentials in the squid giant axon [18]. In contrast, single channel records reveal the gating process itself, i.e. discrete changes in conductance over time.

Generally speaking, experimental studies do not provide clear-cut evidence of ion channel structures and dynamics. This is in part due to the large variability and high plasticity of ion channels, in part to different methods and conditions of measurement. It makes ion channel models tentative by nature. They are developed with reference to particular experimental protocols and conditions. It explains why even basic modeling features are still in dispute, e.g. cooperativity [32][41], and why we still develop methods of measurement. The classical experimental method is to sample voltage and current relationships at discrete steady-state voltages. A recent line of research makes use of dynamic rather than steady-stage voltage to discriminate between voltage-dependent ion channel models [19][23][24][25][26][35][38][39][40][47]. These studies show that ion channels and models can differ substantially under nonequilibrium conditions, even when they share conductance properties in response to steady-state potentials. Since ion channels in vivo are never in a state of equilibrium, this raises the question how to make better use of dynamic conductance for modeling purposes.

The purpose of here is to explore the value of *hysteretic conductance* to

evaluate models of voltage-dependent ion channels. In scientific publications on ion channels, it refers to specific observations of conduction delays in response to voltage change. At the macroscopic level, the hysteretic effect is the conductance loop that arises in response to periodic voltage that matches ion channel kinetics [1][12][42][49][54]. At the microscopic level, ion channel hysteresis refers to an enduring conduction delay that arises in response to voltage change despite steady-state conditions following the change [4][12][45]. In the former case, we face a methodological opportunity, using conductance loops to evaluate ion channel models. In the latter case, we face a theoretical problem in need of explanation. In this article, we use the former to elucidate the latter. The reports on ion channel hysteresis are more or less anecdotal. As far as we know, there has been no explicit discussion of the potential use of hysteretic conductance as support in ion channel modeling.

With "modeling", we here mean formalizing, simulating and evaluating the basic property of voltage-dependent ion channels, i.e. voltage-dependent conductance. The question is how conductance loops and delays can support modeling. A couple of mathematical studies of ion channel hysteresis [14][49] provide a theoretical basis for undertaking such an approach, but to go beyond the most simple of conductance models, the two-state model, we must rely on more informal kinetic modeling and computer simulations. Conductance is then formally equated with *the probability being in an open state*. We make use of a very simple voltage protocol, i.e. the triangular wave-function, and variations of Markov models, to generate hysteretic effects that allow us to systematically map effects to model components.

A Markov model consists of a set of discrete open and closed states, together with a set of rules for state transitions. Ion channel modeling is then a question of (1) defining the state space of ion channels, (2) estimating voltage-dependent rate functions, and (3) testing models against simulation or prediction. The approach is not undisputed [28][29][34][42][50], but it has proven fruitful, being able to summarize data on macroscopic and microscopic levels of observation. We apply the Q-matrix method to simulate conductance models in Matlab [8][9]. We make use of highly idealized models, not restricting the analysis to the kinetics of any particular channel. It makes the argument easy to follow. Of course, we cannot fully account for dynamic conductance by this approach, but it is a start. In real experiments, the translation between ideal and real measures pose methodological challenges that we do not address here.

2 Hysteretic conductance in a two-state model

We start by summarizing the basic formalism of a Markov model of a two-state ion channel, the simplest kind of channel with one open and one closed

state. We rely on transition state theory to define the rate parameters [27].

$$[\mathrm{C}] \underset{\kappa_2}{\overset{\kappa_1}{\rightleftharpoons}} [\mathrm{O}] \tag{2.1}$$

Here $[O]$ denotes the open state, and $[C]$ the closed state. κ_1 and κ_2 are the voltage-dependent transition rates between the states, two parameters in the master equation for the probability of an open state:

$$P_o(t+dt) = P_o(t)(1-\kappa_2 dt) + (1-P_o(t))\kappa_1 dt \tag{2.2}$$

which at equilibrium, steady-state,

$$\frac{P_o(t+dt) - P_o(t)}{dt} = 0 \tag{2.3}$$

gives the stationary open distribution:

$$P_\infty = \frac{\kappa_1}{\kappa_1 + \kappa_2} \tag{2.4}$$

The voltage-dependent rate parameters κ_1 and κ_2 are defined in accordance with transition state theory. We assume that negative potentials favor the closed state, positive potentials the open state, also assuming a linear energy function across the cell membrane:

$$\kappa_1(V) = \kappa_{1/2} e^{+z\delta q_e \frac{(V-V_{1/2})}{kT}} \tag{2.5}$$

$$\kappa_2(V) = \kappa_{1/2} e^{-z(1-\delta) q_e \frac{(V-V_{1/2})}{kT}}, \tag{2.6}$$

where $\kappa_{1/2}$ is the transition rate at the voltage midpoint $V_{1/2}$, when the probabilities of open and closed states are equal (0.5). z denotes the gating charge, δ the voltage sensitivity of forward and backward transitions respectively, q_e the elementary charge, k the Boltzmann's constant, and T the absolute temperature (K). When δ is 0.5, the two transition rates are symmetrical around $V_{1/2}$.

This is the simplest way of formalizing transition rate functions. By assuming non-linear energy landscapes across the cell membrane, we get more flexible rate functions, but also at the cost of an increasing number of parameters [46]. We rest with the simple case.

Combining (2.4), (2.5), and (2.6), we get the Boltzmann version of the stationary open probability distribution:

$$P_\infty = \frac{1}{1 + e^{-z q_e \frac{(V-V_{1/2})}{kT}}} \tag{2.7}$$

The transient probability distribution is derived by integration of equation (2.2), subject to initial conditions $P_o(0) = P_0$ and $P_o(\infty) = P_\infty$:

$$P_o(t) = P_\infty - (P_\infty - P_0)e^{-(\kappa_1+\kappa_2)t}. \tag{2.8}$$

Formula (2.8) expresses the relaxation of the open probability when stepping from one constant voltage to another, i.e. the evolution of open probability after a discrete voltage change, before reaching equilibrium P_∞ at the new voltage. The formula denotes the main component of ion channel models used in the estimation of rate functions κ_1 and κ_2 from macroscopic data.

2.1 Static and dynamic conditions of conductance

In classical electrophysiological experiments — a voltage-clamp study — voltage is changed from one holding potential to another, thereby changing the equilibrium conditions of ion channel conductance, i.e. the open probability. The result is a conductance that *relaxes* towards its new equilibrium. In the case of a two state channel, the curve follows the formula (2.8). This generates a relaxation curve that can be used to estimate rate constants. In single channel studies, a different time series is used for the same purpose. Due to energy fluctuations, single channel conductance goes ON and OFF at random in a discrete manner. By analyzing records of ON (open) and OFF (closed) dwell-time, at different but fixed potentials, we can estimate rate constants as a function of voltage. However, in practice, no method is perfect. Dwell-time series are informative, but more sensitive to perturbation and noise. Relaxation records are less noisy, but more ambiguous. Data can often be fitted to a number of models. Therefore, we should look for complementary ways to analyze voltage-dependent dynamics of ion channels.

The equilibrium condition is a critical assumption in the analysis of both macroscopic and microscopic conductance. However, it is not always clear if and when the equilibrium condition is fulfilled [21][33][42][53]. When it is not, we get conductance depending on both past and present voltage stimulation. With continuous change of voltage, ion channel conductance will never reach equilibrium. The data record is then harder to analyze, since there are in fact no *constants*. Still, some studies demonstrate that important information can be harnessed from nonequilibrium conditions. Recently, dynamic voltage stimulation has been used to generate nonequilibrium conductance effects for the purpose of model discrimination [19][23][24][25][26][35][38][39][40][47]. This line of research has demonstrated that dynamic voltage protocols can reveal more conductance properties of ion channels than static ones.

To use nonequilibrium conditions for modeling purposes, it may be beneficial to begin with the simplest protocols. This is also the case in a handful of studies that explicitly deal with ion channel hysteresis. They rely on

triangular periodic voltage [12][11][49]. The periodic voltage generates conductance loops that allow for systematic measures and comparisons of conductance effects in response to parameter variations. It enables us to identify critical parameters in regulating the voltage sensitivity of ion channels, to map conductance effects onto model parameters. There are a few other studies that also deal with ion channel hysteresis explicitly [1][4][14][45]. The focus is here on theoretical rather than methodological issues. Using discrete voltage protocols, a particular channel, the *Non-Selective Voltage-Dependent Cation* channel (NSVDC), demonstrates large unexplained conductance delays. We come back to this later on.

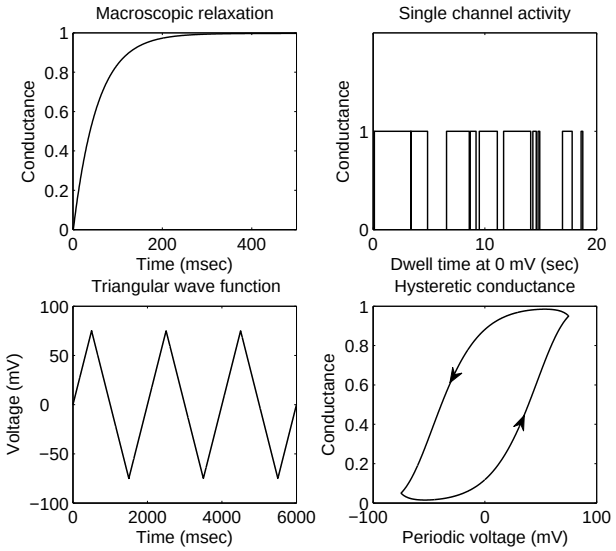

Figure 1: *Three types of conductance generated by simulation of a two state channel with parameters* $k_{1/2} = 1$, $z = 2$, $\delta = 0.5$, $V_{1/2} = 0$. *Upper left: macroscopic relaxation when stepping from* $-75mV$ *to* $+75mV$. *Upper right: single channel dwell time in open (1) and closed (0) states. Lower left: triangular wave used to simulate hysteretic conductance. Lower right: hysteretic conductance at the third period of the periodic triangular voltage, starting at 0, with speed 300mV/second. In all our model simulations, a single wave consists of 2000 discrete voltage steps, with constant relaxation time for all steps. The time period of the wave is the sum of the relaxation time for all wave steps. The hysteretic effect is defined by the normalized loop area (0 < loop area < 1)*

In figure (1), we illustrate the three types of conductance data that we deal with in this article: (1) the relaxation record, (2) dwell-time series, and (3) hysteretic conductance (conductance loops). The plots show con-

ductance in the two-state model. The parameters z, δ, $V_{1/2}$, and $\kappa_{1/2}$ have been set to 2, 0.5, 0, and 1. At a particular voltage, depending on the direction of voltage change, the hysteretic conductance is higher or lower than its value at equilibrium. This is even more clear in figure (2), where hysteretic conduction is a function of the ramp speed of voltage change. At very slow speed, the channel has time to reach equilibrium, and we get no hysteretic effect. At very high speed, the ion channel has no time to adapt to voltage changes, for which reason the conductance converges to its value at the midpoint of the voltage range.

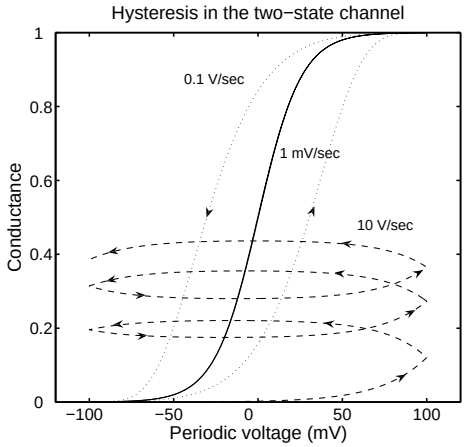

Figure 2: *Hysteretic conductance in a two-state channel, with periodic voltage between −100 and +100 mV, starting at −100mV, with parameters* $k_{1/2}$ *= 1,* $z = 2$*,* $\delta = 0.5$ *and* $V_{1/2} = 0$*. At slow speed, 1 mV/s, there is enough time to reach equilibrium of open probability at each step of voltage change. At fast speed, 10V/s, the change in open probability is lagging behind the voltage change and converges to a loop around open probability 0.5.*

2.2 Analytical theory of hysteresis in a two-state channel

Pustovoit et al [49] have formalized an analytical theory of hysteresis for the two-state model of ion channels. They define hysteresis as *the loop area of conductance generated by triangular voltage change with period T and unit amplitude* (c.f. figure (2)). They derive formulas for the explicit calculation of the periodic asymptotic open probability, as well as formulas for the calculation of the loop area. In the following, we summarize the theory. The derivation here is a highly condensed version of the original. We refer to the original article for details.

Voltage V is assumed to be deterministic and periodic:

$$V_T(t+T) = V_T(t) \tag{2.9}$$
$$V_T(t) = \Delta V \varphi_T(t) \tag{2.10}$$
$$V(t) = H(t)V_T(t) \tag{2.11}$$

where $V_T(t)$ a periodic function with period T and amplitude ΔV, $\varphi_T(T + t) = \varphi_T(t)$ a periodic function with period T and unit amplitude, and $H(t)$ the Heaviside function.

Since the rate functions are voltage dependent, periodic voltage implies time-dependent rate functions: $\kappa_1(t)$ and $\kappa_2(t)$. The modified master equation for a two-state channel follows.

$$P_o(t+dt) = P_o(t)(1-\kappa_1(t)dt) + (1-P_o(t))\kappa_2(t)dt \tag{2.12}$$
$$P_o(t) = P_o(t_0)e^{-\int_{t_0}^{t}(\kappa_1(t_1)+\kappa_2(t_1))dt_1} + \int_{t_0}^{t}\kappa_2(t_1)e^{-\int_{t_1}^{t}(\kappa_1(t_1)+\kappa_2(t_1))dt_2}dt_1 \tag{2.13}$$

To derive a formula for the asymptotic periodic probability $P_\infty(t)$, equation (2.13) is conditioned on the period n. $P_o(nT)$ is then substituted for $P_o(t_0)$ in (2.13):

$$P_o(t|n) = P_o(nT)e^{-\int_{nT}^{t}(\kappa_1(t_1)+\kappa_2(t_1))dt_1} + \int_{nT}^{t}\kappa_2(t_1)e^{-\int_{t_1}^{t}(\kappa_1(t_2)+\kappa_2(t_2))dt_2}dt_1 \tag{2.14}$$

To derive the limit of $P_o(nT)$ in (2.14), $n \to \infty$, equation (2.13) is rewritten as a recursion formula:

$$P_o((n+1)T) = \gamma P_o(nT) + a_0 \tag{2.15}$$

where γ and a_0 refer to

$$\gamma = e^{-\int_0^T(\kappa_1(t)+\kappa_2(t))dt} \tag{2.16}$$

and

$$a_0 = \int_0^T \kappa_2(t_1)e^{-\int_{t_1}^{T}(\kappa_1(t_2)+\kappa_2(t_2))dt_2}dt_1 \tag{2.17}$$

$P_o(0)$ is the equilibrium open probability in the absence of voltage, V(0)=0.

$$P_o(0) = \kappa_1(0)/(\kappa_1(0)+\kappa_2(0)) \tag{2.18}$$

With this initial condition, the limit of P(nT) is calculated and substituted for P(nT) in equation (2.13),

$$\lim_{n\to\infty} P_o(nT) = \frac{a_0}{1-\gamma} \tag{2.19}$$

which gives us a formula for the asymptotic probability:

$$P_{o,\infty}(t) = \lim_{n\to\infty} P(t|n) = \frac{a(t)}{1-\gamma} \tag{2.20}$$

where a(t) is given by

$$a(t) = \int_t^{t+T} \kappa_2(t_1) e^{-\int_{t_1}^{t+T}(\kappa_1(t_2)+\kappa_2(t_2))dt_2} dt_1 \tag{2.21}$$

Equation (2.20) allows us to calculate the periodic, asymptotic open probability of a two-state channel with period T. Pustovoit et al [49] also derive an equation for calculating the magnitude of hysteresis (A(t)), the so called "loop area":

$$A(T) = \int_0^{T/2} P_\infty(t)|\dot{V}_T(t)|dt - \int_{-T/2}^{0} P_\infty(t)|\dot{V}_T(t)|dt \tag{2.22}$$

Hysteresis is here formalized by *the integral of the difference in conductance during hyperpolarization (first term) and depolarization (second term).* It is a sum over the periodic voltage range translated into its time domain.

Pustovoit et al [49] demonstrates that the hysteresis goes to zero when the period goes to zero or to infinity. Several factors interact to set the magnitude in between: the amplitude, the period, and the rate functions. Hysteresis increases with amplitude, end even if explicit derivation is lacking, optimal interaction takes place when the period and the rate constants are of the same order of magnitude.

The analytical model of hysteresis in ion channels demonstrates that periodic voltage generates periodic conductance. The probability of being in the open state will then depend on the present voltage input and its direction of change. To discuss its value for electrophysiological and empirical models of ion channel conductance, we will translate it into more traditional kinetic terms.

3 Kinetic factors in conductance loops

For the rate functions κ_1 and κ_2 (2.5-2.6), z defines the voltage-sensitivity of the ion channel. In real channels, the voltage-sensitivity is determined by a corresponding set of charged residues that react to changes in voltage potential, promoting conformational changes of the protein that generate discrete change of conductance (ON/OFF) [52]. The parameter z summarizes the responsiveness to voltage change. Since an increase in charge is equal to an increase in amplitude, hysteretic conductance effects increase with z.

The parameter z is the main kinetic factor in generating conductance loops. In contrast, the voltage midpoint $V_{1/2}$ sets the center of the hysteretic conductance. At $V_{1/2}$, the conductance function is steepest, whereas the

relaxation time is at its maximum, favoring hysteresis. If the center of periodic voltage V_c deviates from $V_{1/2}$, reduction of hysteretic effects follows.

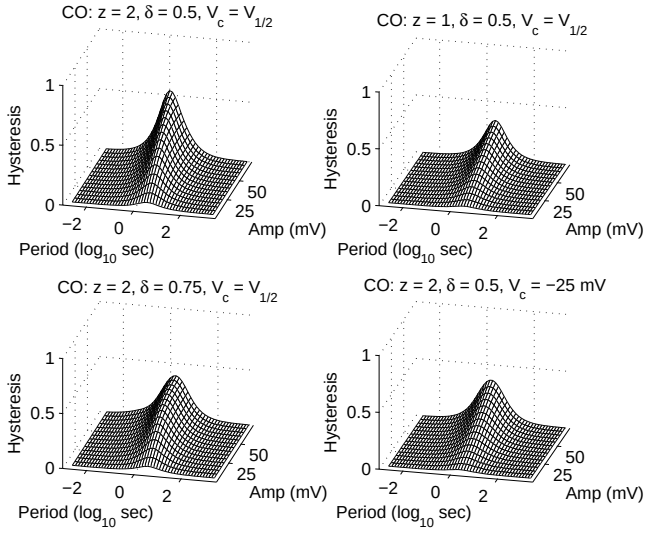

Figure 3: *Hysteretic conductance is the stationary (stable) conductance loop area with respect to period and amplitude of periodic voltage stimulation, i.e. the triangular wave function. A single triangular wave consists of 2000 discrete voltage steps, with constant relaxation time for all steps. The time period (log_{10} seconds in figure) is the log_{10} sum of the relaxation time for all steps in the wave. Upper left: standard parameter values, $z = 2$, $\delta = 0.5$, $V_{1/2} = 0$, and $\kappa_{1/2} = 1$. Upper right: charge reduction, $z = 1$. Lower left: charge asymmetry, $\delta = 0.75$. Lower right: wave displacement with respect to the voltage midpoint of activation $V_{1/2}$, $V_c = -25mV$. When parameter values deviate from optimal conditions (maximal z, $\delta = 0.5$ and $V_c = V_{1/2}$), hysteresis is reduced.*

δ and $\kappa_{1/2}$ relate to z and $V_{1/2}$ respectively. δ defines the symmetry of the voltage-sensor. Hysteresis is maximal when the gating charge is symmetrically distributed, $\delta = 0.5$, making ion channel conductance equally responsive to hyperpolarization and depolarization around $V_{1/2}$. Asymmetrical rate functions, i.e. $\delta \neq 0.5$, result in asymmetrical time constants below and above $V_{1/2}$, implying different optimal voltage periods for maximal hysteresis, and lowering the hysteresis compared to symmetrical rate functions. Finally, $\kappa_{1/2}$, together with $V_{1/2}$, limits the range of effective voltage frequencies. In figure 3, we render the results of four simulations of the two-state channel illustrating the effects of parameter values on hysteresis, i.e. conductance loop areas. When the parameter values deviate from ideal conditions, i.e. lower z, $V_c \neq V_{1/2}$, and $\delta \neq 0.5$, hysteresis is reduced.

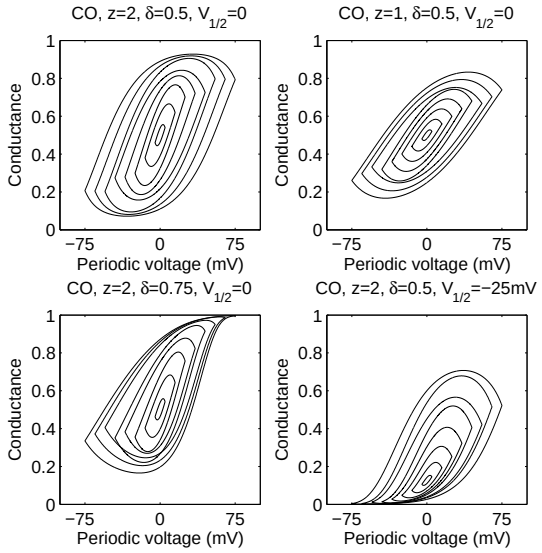

Figure 4: *"Conductance fingerprints". The graphs show the maximal conductance loops in response to periodic voltage of amplitudes 5, 15, 25, 35, 45, 55, 65, and 75 mV (from inner to outer curves). The time period for maximal conductance varies depending on amplitude (cf. figure 3). Each loop corresponds to a singular triangular wave. Upper left: standard parameter values. Upper right: charge reduction,* $z = 1$*. Lower left: charge asymmetry,* $\delta = 0.75$*. Lower right: midpoint displacement,* $V_{1/2} = -25mV$*.*

The loop area is a rough measure of the responsiveness of the model to voltage change. It can also be informative to look at the geometry of the conductance loops at particular amplitudes and periods. Figure 4 renders the conductance loops of maximal hysteresis at amplitudes 5, 15, 25, 35, 45, 55, 65, and 75 mV (from inner to outer curves), the periods varying about 1-5 ms depending on the amplitude. These sets of loops resemble fingerprints, demonstrating rather striking changes in hysteretic conductance depending on changes in parameter values. For δ and $V_{1/2}$, deviations from ideal values attenuate hysteresis, but in ways depending on the parameter in question.

A reduction in z results in a general reduction of conductance loops and hysteresis, whereas the asymmetrical conditions generate asymmetrical conductance loops, each pattern depending the parameter and its value. Thus, conductance loops may indicate and/or confirm distinct features of voltage-dependent rate functions, especially when combined with data records on relaxation and dwell-time.

3.1 Hysteretic conductance in multi-state channels

In this section, we extend the discussion to models with more than two states, with the aim of assessing the potential use of hysteretic conductance in exploring the state space and voltage-dependent kinetics. We make minimal extensions to keep the simulations simple and the arguments easy to follow. The discussion is restricted to two idealized Markov models representing two important types of state space: independent versus cooperative gating (3.1 and 3.2) [2][16][27][56]. Our aim is to test whether hysteretic conductance can serve to reveal critical features of these Markov models.

In the original study of action potentials by Hodgkin and Huxley, ionic conductances are assumed to be regulated by a number of conductance "particles". Each particle takes two values, active (ON) or not (OFF), with a probability depending on the voltage potential. The numbers and types of particles vary depending on the conductance in question, e.g. four activation particles for the potassium conductance G_K, three for the sodium conductance G_{Na}. When all particles are in their active state, the channel conductance changes from 0 to 1. In some cases, we must also deal with inactivation particles that block the conductance after depolarization, e.g. the sodium conductance G_{Na}. Here we restrict the discussion to models with activation alone, the potassium conductance.

We let two premises govern the kinetics of HH gating particles. First, each gating particle responds to voltage changes independently of each other. Secondly, the same rate functions govern all activation particles. These premises allow us to model the independent activation pathway by the Markov scheme (3.1), with linear addition of activation and deactivation rates when going between closed and open states, i.e. a fourfold increase for four closed particles, threefold increase for three closed particles, etc.

$$[C_1] \underset{\kappa_4}{\overset{4\kappa_3}{\rightleftharpoons}} [C_2] \underset{2\kappa_4}{\overset{3\kappa_3}{\rightleftharpoons}} [C_3] \underset{3\kappa_4}{\overset{2\kappa_3}{\rightleftharpoons}} [C_4] \underset{4\kappa_4}{\overset{\kappa_3}{\rightleftharpoons}} [\mathrm{O}] \tag{3.1}$$

An alterative hypothesis to independent gating is that ion channels consist of protein subunits that respond in a cooperative manner to voltage change, i.e. the activation of a single subunit increases the activation rates of the remaining subunits. In contrast to the HH scheme, where the condition of independence imposes strict rules for relations between rate constants, Markov schemes for cooperativity can take many and different forms. However, to keep the comparative analysis clear, we choose the most stereotyped case, a simple reversal of the rate modifiers for independent gating, which gives us the cooperative scheme (3.2). Each successive activation and deactivation step, from $[C_i]$ to $[C_{i+1}]$, or from $[\mathrm{O}]/[C_i]$ to $[C_4]/[C_{i-1}]$, increases the transition rate.

$$[C_1] \underset{4\kappa_6}{\overset{\kappa_5}{\rightleftharpoons}} [C_2] \underset{3\kappa_6}{\overset{2\kappa_5}{\rightleftharpoons}} [C_3] \underset{2\kappa_6}{\overset{3\kappa_5}{\rightleftharpoons}} [C_4] \underset{\kappa_6}{\overset{4\kappa_5}{\rightleftharpoons}} [\mathrm{O}] \tag{3.2}$$

To evaluate the effects of the two transition schemes on hysteretic conductance, we use default parameter values for z, δ, and $\kappa_{1/2}$ ($z = 2$, $\delta = 0.5$ and $\kappa_{1/2} = 1$), and normalized values for midpoints of activation $V_{1/2}$. In multistate models, $V_{1/2}$ depends on both the number of states and the type of state transitions. For the independent model, we can rephrase the Boltzmann formula and derive the midpoint explicitly:

$$V_{1/2} = -\frac{kT}{ze_0} log\left(-1 + \left(\frac{1}{2}\right)^{-\frac{1}{4}}\right), \tag{3.3}$$

which gives $V_{1/2} = 21.4$ mV. For the cooperative model, we use numerical approximation, which gives $V_{1/2} = 2.2$ mV.

Figure 5 renders maximal conductance loops of independent and cooperative versions of the CCCCO model at different amplitudes of periodic triangular voltage. Compared to the two-state model (figure 3), both versions display asymmetrical effects, with larger lags at hyperpolarized potentials, which agrees with a larger delay in activation due to multiple closed states. The asymmetry is most apparent at larger amplitudes, and more clearly expressed for cooperative subunits. By themselves, the conductance loops do not appear to provide any clear-cut information on gating schemes, independent versus cooperative models. To put them to better use, we need to relate them to conductance curves at equilibrium.

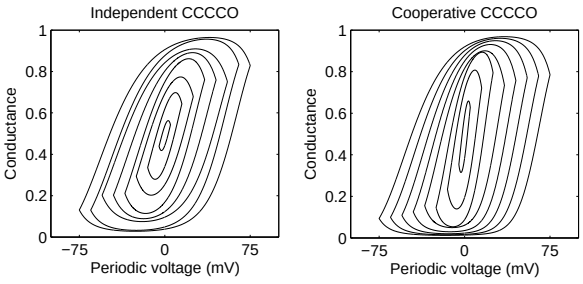

Figure 5: *Maximal conductance loops for independent and cooperative CCCCO for periodic voltage of different amplitudes: 5, 15, 25, 35, 45, 55, 65, and 75 mV (from inner to outer curves). The time period for maximal conductance varies depending on amplitude (cf. figure 6). Compared to the two-state model, more closed states result in larger hysteretic loops. Cooperativity reinforces the effect.*

Compared to the independent model, the cooperative model has a steeper conductance curve at equilibrium (cf. dashed line compared to full line in top left plot of figure 6). This is a well-known property of cooperativity in enzymatic reactions and biochemical systems [56]. Cooperativity involves steeper sigmoidal functions, forming sharper activation thresholds. However,

steepness does not necessarily imply cooperativity. For voltage-dependent channels, the gating charge "z" is the more effective contributor to steepness or sharpness. It is illustrated by the dotted line in the top left plot of figure 6. The line represents an independent four-state model where z is set to 4.18, which corresponds to the slope of the curve of the cooperative model (derivation below). Thus, the voltage sensitivity of conductance at equilibrium is effected by both gating scheme and gating charge, which renders these curves ambiguous regarding their nature.

In figure 6, we render the three surface plots of multistate hysteretic conductance with respect to period and amplitude for three models: (1) independent (top right) (2) cooperative (lower left) and (3) adjusted independent (lower right). In the latter model, the gating charge has been adjusted to match the slope of activation of the cooperative model. The charge adjustment is derived from the Boltzmann formula. For the independent model with n gating particles, we match the conductance at equilibrium to the conductance of the cooperative model at voltage shift ΔV from midpoint $V_{1/2}$. The formula is the following:

$$z_{adj} = \frac{kT}{\Delta V e_0} \left(log \left(-1 + \left(\frac{1}{2} \right)^{-\frac{1}{n}} \right) - log \left(-1 + (p_o)^{-\frac{1}{n}} \right) \right). \qquad (3.4)$$

Setting ΔV to +10 mV, and p_o to 0.8641 according to numerical results for the cooperative model, we get $z_{adj} = 4.18$ for the adjusted model. The surface plots show two features. With matching gating charge, the hysteretic effect for the independent model increases with the amplitude of the periodic voltage, but remains low at low amplitudes. Furthermore, there is an interaction effect for the adjusted model, a displacement of the hysteretic effect at larger amplitudes towards higher frequencies. Thus, given conductance curves at equilibrium, hysteretic conductance provides indications of independent and cooperative gating schemes. When gating charge is known, the support of hysteretic conductance for modeling purposes gets even stronger.

To check if these observations hold more generally, we extend the comparisons to 3-, 4- and 6-state models. The basic principles of the gating schemes (3.1) and (3.2) remain the same, except for the number of states and the rate factors that go with this. For example, rate factors are 1 and 2 for a 3-state model; and 1, 2, 3, 4 and 5 for a 6-state model. We reuse default parameter values. Figure 7 shows plots of conductance curves of all the models at equilibrium. To define adjusted models, we increase the gating charge of the independent models. Using $\Delta V = 10$ mV is an arbitrary choice. Matching conductance slopes at smaller voltage shifts generates larger differences between independent and cooperative models. For comparison, we keep $\Delta V = 10$ mV.

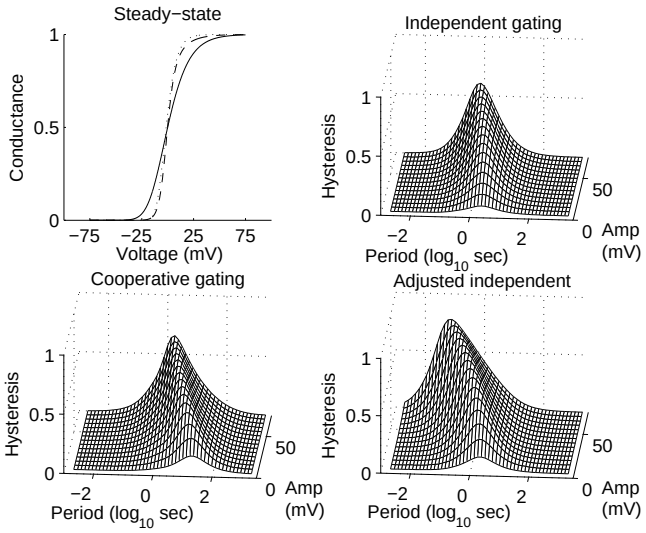

Figure 6: *Hysteretic conductance of independent and cooperative four-state models (CCCCO). Top left: stationary conductance of independent model (full line) and cooperative model (dashed line) with default parameter values:* $z = 2$, $\delta = 0.5$ *and* $\kappa_{1/2} = 1$, *and with voltage midpoints of activation* $V_{1/2}$ *adjusted to zero (0.0214 and 0.0022 respectively). The dotted line represents the conductance of a charge adjusted independent four-state model,* $z = 4.18$, *matching the conductance of the cooperative gating scheme at equilibrium. The three surface plots show the hysteretic conductance generated for the three models, i.e. the conductance loop area with respect to the period (seconds in* log_{10}*) of the triangular wave and its amplitude (mV).*

To summarize the simulation results we make use of maximal hysteretic conductance, i.e. the maximal loop area at a given amplitude of periodic voltage. The period that generates maximal hysteretic effect depends on amplitude, varying between 1-5 ms. In figure 8, we render three scatter plots for independent, cooperative and adjusted models respectively. The pattern observed for the 4-state models is confirmed. Independent models demonstrate slow gradual increase of hysteretic conductance with amplitude. Increased gating charge does not alter this pattern. It actually reinforces it, reducing hysteretic conductance at smaller amplitudes and increasing it at larger amplitudes. In contrast, the increase in hysteretic effect of cooperative models is most marked at intermediate amplitudes.

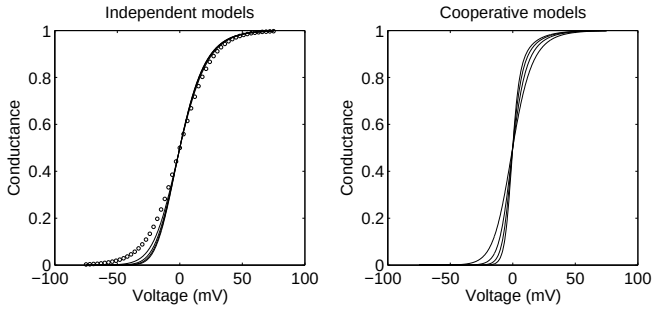

Figure 7: *Conductance curves of independent and cooperative models at equilibrium. Left plot: Small circles represent the conductance curve of the two-state model (CO). Full lines represent conductance curves of independent 3-/4-/5-/6-state models. Right plot: lines represent conductance curves of cooperative 3-/4-/5-/6-state models. To adjust conductance curvatures of independent models to curvatures of cooperative models, gating charge is increased according to the formula (composite Boltzmann):* $z_{adj} = \frac{kT}{\Delta V e_0}\left(log\left(-1+\left(\frac{1}{2}\right)^{-\frac{1}{n}}\right) - log\left(-1+(p_o)^{-\frac{1}{n}}\right)\right)$*, where* ΔV *is a chosen voltage shift (+10 mV) from the midpoint of activation* $V_{1/2}$*, and* p_o *is the conductance at the corresponding voltage shift in the cooperative model.*

3.2 Assessing rate functions

Under the HH condition of independent gating, records on conductance loops may be used to directly estimate rate functions. We rewrite the master equation of the two state channel (2.2):

$$[\dot{\mathrm{O}}]_1 = \kappa_1(\mathrm{V})[\mathrm{C}]_1 - \kappa_2(\mathrm{V})[\mathrm{O}]_1 \tag{3.5}$$

$$[\dot{\mathrm{O}}]_2 = \kappa_1(\mathrm{V})[\mathrm{C}]_2 - \kappa_2(\mathrm{V})[\mathrm{O}]_2 \tag{3.6}$$

$$\Leftrightarrow$$

$$\kappa_1(\mathrm{V}) = \frac{[\dot{\mathrm{O}}]_1 + \kappa_2[\mathrm{O}]_1}{[\mathrm{C}]_1} = \frac{[\dot{\mathrm{O}}]_1 + \kappa_2[\mathrm{O}]_1}{(1\text{-}[\mathrm{O}]_1)} \tag{3.7}$$

$$\kappa_2(\mathrm{V}) = \frac{[\dot{\mathrm{O}}]_1[\mathrm{C}]_2 - [\dot{\mathrm{O}}]_2[\mathrm{C}]_1}{[\mathrm{O}]_2[\mathrm{C}]_1 - [\mathrm{O}]_1[\mathrm{C}]_2} = \frac{[\dot{\mathrm{O}}]_1(1\text{-}[\mathrm{O}]_2) - [\dot{\mathrm{O}}]_2(1\text{-}[\mathrm{O}]_1)}{[\mathrm{O}]_2(1\text{-}[\mathrm{O}]_1) - [\mathrm{O}]_1(1\text{-}[\mathrm{O}]_2)} \tag{3.8}$$

where the dot marks the time derivative of open probability, and indices 1 and 2 mark the two data points on the conductance loop at a particular voltage potential during hyperpolarization and depolarization respectively.

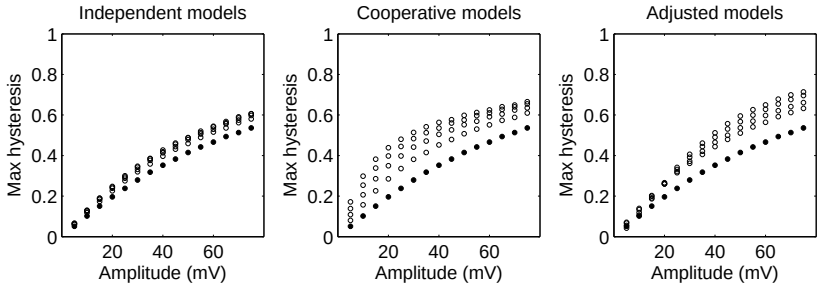

Figure 8: *Maximum hysteresis of independent, cooperative and adjusted independent models. Maximum hysteresis is the maximum loop area with respect to the amplitude of the triangular wave: 5, 15, 25, 35, 45, 55, 65, and 75 mV. The period differs depending on the amplitude: 1-5 mV. For comparison, the three plots also represent the maximum hysteresis of the two state model (the lower filled circles in each plot). The open circles represent maximum hysteresis of 3-/4-/5-/6-state models. The size of the model relates linearly on the level of the circle. Successive models in size are represented by successive circles in vertical direction. For the charge adjusted models, there is an interaction effect. Larger models result in larger hysteresis at larger amplitudes, but lower hysteresis at lower amplitudes. The scatter plots show that the differences between independent and cooperative gating schemes remain after adjusting for gating charge. For independent models, there is a gradual increase in hysteretic conductance with amplitude, whereas cooperative models favor rapid increase at lower amplitudes. Adjustment of gating charge reinforces these differences.*

For a simple two-state voltage-dependent channel, a record of hysteretic conductance at a single amplitude and period will be sufficient to estimate rate functions. At each potential, we have two data points, the open probability and its derivative, which provide us with an explicit solution of the rate equations without resorting to numerical solutions. A necessary condition for this estimation is that the conductance never reaches a state of equilibrium, in which case the rate equations become indeterminate. Another condition is the quality of the experimental data, i.e. high precision in measurements, low noise levels. Here we simply assume that these conditions can be met in some way, e.g. by averaging over several experiments or frequencies.

In a two state-channel, the open probability dictates the probability of being in the closed state. This makes estimation easy. For multi-state ion channels with more free parameters, data points are in general insufficient to solve the rate equations. However, assuming HH modeling conditions, independent gating particles and identical rate functions, we may still estimate

the rate functions explicitly, which may at least serve to test the assumption of independent and identical gating particles.

For a multi-state HH model with n gating particles, the open probability is given by the product of the open probabilities of the particles. Assuming identical parameter values for each gating particle, we may calculate the open probability of the multistate model $[O]_n$ by replacing $[O]$ and $[\dot{\mathrm{O}}]$ in the two-state formula by the corresponding multistate variables.

$$[\mathrm{O}]_n = [\mathrm{O}]^n \tag{3.9}$$

$$[\dot{\mathrm{O}}]_n = \mathrm{n}[\mathrm{O}]^{n-1}[\dot{\mathrm{O}}] \tag{3.10}$$

4 Mode shifts and conductance delays

In a series of studies of the hyperpolarization-activated channel (HCN), alternative Markov models were compared on the basis of the triangular wave protocol, as well as traditional relaxation protocols [12][11]. One also checked conductance loops of the potassium (K) channel. For both HCN and K channels, the hysteretic effect was less pronounced for the ion channel than for the model. The loop area was smaller and more stable over a broad range of frequencies. The models predicted larger effects. The discrepancy agrees with studies of nonequilibrium conductance. As mentioned earlier, there are studies using dynamic voltage protocols for the purpose of model discrimination. Even if not explicitly stated, the published data indicates lower sensitivity to frequency variation in real channels compared to models [26][38]. In other words, models based on relaxation protocols overestimate ion channel sensitivity to frequency variation. Thus, voltage-dependent Markov models appear to lack some property that makes it difficult to fit them to dynamic data. Here we explore a line of inquiry suggested by the HCN studies, that can be explored with conductance loops.

4.1 Mode-shifts in HCN

Hyperpolarization-activated cyclic nucleotide-gated cation channels (HCN) support the I_h current, the "pacemaker current", also referred to as I_f in the heart and I_q in the brain. As its name reveals, it activates at hyperpolarization and closes at depolarization. It is modulated by cAMP, as CNG channels, shifting the midpoint of activation towards depolarized potentials. It appears to have multiple closed and open states. Furthermore, the channel is permeable to both K^+ and Na^+ ($\approx$ 4:1), to some extent also Ca^{+2} [36]. The voltage midpoint is about $-70/-90$ mV. The single channel conductance is low, 1-10 pS, which is the main obstacle for patch-clamp studies of single channel activity. The kinetics varies depending on channel subtype

[3][55]. Several, but non-conclusive Markov models have been proposed to account for the kinetics [10].

Two isoforms of HCN channels demonstrate hysteresis, spHCN and HCN1. The hysteretic effect involves shifts in the voltage dependency of both gating currents and the macroscopic conductance depending on holding potential. The midpoints of activation are shifted about +(40-60) mV when measured from hyperpolarized holding potentials compared depolarized potentials. It goes together with other changes of kinetics. To account for all observations, a distinct mechanism is proposed for regulating the voltage-sensitivity of the HCN channel, *mode-shift*. It is assumed to involve two modes with different midpoints of activation. Mode I has a voltage midpoint of activation at -105 mV; and mode II at -45 mV. With an average midpoint of activation at -75 mV, the mode shift is $\pm$ 30 mV. The effect is a voltage-independent resistance to conductance change, i.e. transitions between open and closed states.

To formalize mode shift, the authors make use of a circular four-state model. To avoid details on HCN kinetics, we present a generalized model.

$$\begin{array}{ccc} [C_2] & \underset{\frac{\kappa_2}{f}}{\overset{\kappa_1 f}{\rightleftharpoons}} & [O_2] \\ \frac{\lambda}{f} \uparrow\downarrow \lambda f & & \lambda f \uparrow\downarrow \frac{\lambda}{f} \\ [C_1] & \underset{\kappa_2 f}{\overset{\frac{\kappa_1}{f}}{\rightleftharpoons}} & [O_1] \end{array} \tag{4.1}$$

To keep comparisons with previous models and simulations clear, we let the circular model open and close at depolarization and hyperpolarization respectively. Thus, we make use of κ_2 and κ_1. The mode shift is made explicit by λ, the voltage-independent mode transition rate, and an allosteric factor f, modulating the mode transition rate depending on the conductance state. The allosteric factor also secures the condition of micro-reversibility for circular models at equilibrium. One implication of the structure is a stationary distribution of open probability equal to the one of the two-state channel. This is clear from the following derivation.

$$
\begin{aligned}
\mathrm{P}([\mathrm{O}]) &= \frac{[\mathrm{O}_1] + [\mathrm{O}_2]}{[\mathrm{O}_1] + [\mathrm{O}_2] + [\mathrm{C}_1] + [\mathrm{C}_2]} && (4.2)\\
\mathrm{P}([\mathrm{O}]) &= \frac{\frac{[\mathrm{O}_1]}{[\mathrm{C}_1]} + \frac{[\mathrm{O}_2]}{[\mathrm{O}_1]}\frac{[\mathrm{O}_1]}{[\mathrm{C}_1]}}{\frac{[\mathrm{O}_1]}{[\mathrm{C}_1]} + \frac{[\mathrm{O}_2]}{[\mathrm{O}_1]}\frac{[\mathrm{O}_1]}{[\mathrm{C}_1]} + \frac{[\mathrm{C}_1]}{[\mathrm{C}_1]} + \frac{[\mathrm{C}_2]}{[\mathrm{C}_1]}} && (4.3)\\
\mathrm{P}([\mathrm{O}]) &= \frac{\frac{\kappa_1}{\kappa_2 f^2} + \frac{\kappa_1}{\kappa_2}}{\frac{\kappa_1}{\kappa_2 f^2} + \frac{\kappa_1}{\kappa_2} + 1 + \frac{1}{f^2}} && (4.4)\\
\mathrm{P}([\mathrm{O}]) &= \frac{1}{1 + \frac{\kappa_2}{\kappa_1}} && (4.5)\\
&= \frac{\kappa_1}{\kappa_1 + \kappa_2}
\end{aligned}
$$

Thus, the open probability at equilibrium is equal to a two-state channel, where the open probability only depends on κ_1 and κ_2. The equality is due to highly idealized conditions: (1) symmetric transition rates, (2) the symmetric allosteric factor λ, (3) and symmetric mode transition rates. Although unrealistic, it allows us to simulate and compare the hysteretic effect of mode shifting as a distinct gating scheme, like independent and cooperative gating schemes.

Figure 9 shows the simulation results for the four-state channel, with f=2.175, corresponding to a mode-shift $\approx$ 40 mV ($\approx \pm$20 mV from the midpoint of activation). The two surface plots render results for mode transition rates 1 Hz and 0.1 Hz respectively. The remaining parameters have default values: $V_{\frac{1}{2}} = 0$, $\kappa_{\frac{1}{2}} = 1$, $z = 2$, and $\delta = 0.5$. Compared to the two state channel, the mode-shift reduces maximal hysteresis and broadens the range of effective frequencies, in particular for the model with lower mode transition rate. Even if not explicitly stated, this is what was observed in the HCN study. The result is also in line with the studies indicating that the effect of frequency variation on ion channels is more limited than expected from classical models.

With mode-shifting, the hysteretic effect, delayed conductance, is a structural property of ion channels. It is an intrinsic voltage-independent switch of kinetics delaying voltage-dependent transitions. It goes beyond nonequilibrium conditions of dynamic voltage. Recent research on the voltage-sensor of ion channels (S4) indicates that the mode-shifting is a general property of voltage-dependent channels [54]. The basic mechanism is the same, but the conductance effects vary depending on overall ion channel kinetics. In the final sections, we propose that mode shifting may also explain more exceptional cases of single channel hysteresis.

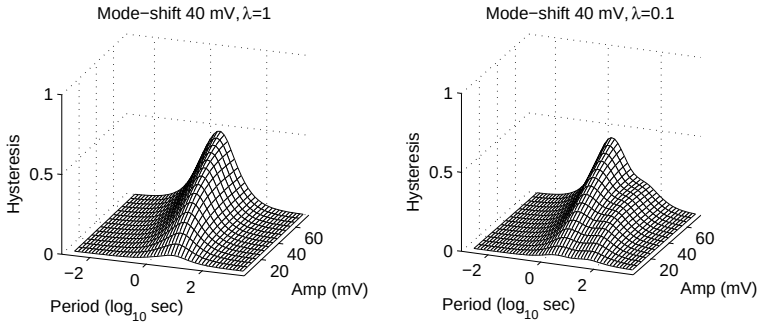

Figure 9: *Hysteresis in the circular four-state model, with allosteric factor f=2.175, corresponding to a mode-shift* ± 20 *mV: Compared to the two-state model, mode-shifting attenuates the maximum and broadens the effective range of frequencies in response to which hysteretic conductance is generated. This is most prominent for mode shifting with lower mode transition rate than voltage-dependent rates. Left:* $\lambda = 1$*. Right:* $\lambda = 0.1$*.*

4.2 Hysteresis in NSVDC

The *Non-Selective Voltage-Dependent Cation* (NSVDC) channel is a channel found in the human red blood cell (RBC) membrane [4][5][22]. The channel is permeable to both mono- and divalent cations and contributes to depolarization, like the HCN channel. In both macroscopic and microscopic studies, the channel demonstrates a pronounced delay of conductance after discrete voltage change. When stepping from a hyperpolarized potential (0 mV) to a depolarized one, the open probability is markedly lower than when stepping to the same potential from an even more depolarized potential (activation midpoint shift about 25 mV). This holds after long periods of measurement (hours). The authors conclude that the enduring effect was long and stable enough to exclude non-equilibrium effects on conductance [22].

In response to the experimental findings, Gudowska-Nowak et al [14] proposed a stochastic theory of hysteresis in single channels. It predicts hysteresis as a general property of ion channels, for which reason it deserves attention. Let us briefly summarize it.

$$V(T) = \langle V \rangle + \xi(t) \tag{4.6}$$

Voltage $V(t)$ is assumed to be random and time-dependent due to voltage fluctuations $\xi(t)$ defined by a Gaussian stochastic process (Wiener process). This transforms the gating function of a two state channel — the master equation (2.2) — into a stochastic differential equation, making the open probability into a random variable itself. The open probability will not only depend on the applied voltage potential, but also on the slow time evolution

of the open probability distribution.

$$\langle \xi(t)\xi(t+s)\rangle = \sigma^2 e^{(-s/\epsilon)} \tag{4.7}$$

where ϵ is the autocorrelation time.

The model presupposes that the rate of voltage fluctuation, ξ, is much slower than the equilibration time of the channel, τ. The open probability p_∞(V) is then both random and quasi-stationary, with a probability density $p_s(p_o)$ that under quasi-stationary conditions is derived from the density of ξ:

$$p_s(\xi) = \frac{1}{\sqrt{2\pi}\sigma} e^{-\frac{\xi^2}{2\sigma^2}} \tag{4.8}$$

By substituting rate functions (2.5) and (2.6) for rate constants in formula (2.4), we derive a stationary open probability function of voltage.

$$p_\infty(V) = \frac{1}{1+e^{-c(V-V_{1/2})}} \tag{4.9}$$

where c is a constant.

By using formula (4.6) and substituting $\xi + \langle V\rangle$ for V, p_∞ is made a function of ξ. Standard probabilistic calculus is applied to derive the density $P_s(p_\infty)$:

$$P_s(p_\infty) = p_s(f^{-1}(p_\infty))|\frac{d}{dp_\infty} f^{-1}(p_\infty)| \tag{4.10}$$

$$= \frac{1}{\sqrt{2\pi}\sigma c}\frac{1}{p_\infty(1-p_\infty)} e^{-\frac{(V_{1/2}+\frac{1}{c}log(\frac{p_\infty}{1-p_\infty})-\langle V\rangle)^2}{2\sigma^2}} \tag{4.11}$$

Figure 10 illustrates the density of open probability for different parameter values, σ^2 and voltage potentials $\Delta V = V_{1/2} - \langle V\rangle$. For $\sigma^2 > 1$, the density (4.10) is bimodal. The density has maximums at $p_0 = 0$ and 1, minimum in between. Gudowska-Nowak et al [14] concludes that hysteresis is induced by continuous change of voltage potential ΔV.

The stochastic theory predicts hysteresis when the voltage fluctuation is above a critical value, $\sigma^2 = 1$. However, this is based on a rather questionable assumption. The parameter values $c = 1$ and $\Delta V = 1$ is within physiological conditions, $|\Delta V| \approx 50$ mV, but assuming voltage fluctuations of the same order of magnitude is extraordinary. Furthermore, the cited findings point rather to voltage-independent hysteresis, delayed conductance over enduring conditions. Finally, the theory predicts a bimodal density of open probability for all voltage-dependent channels. However, reports are scarce. Let us therefore propose an alternative mechanism to explain the findings.

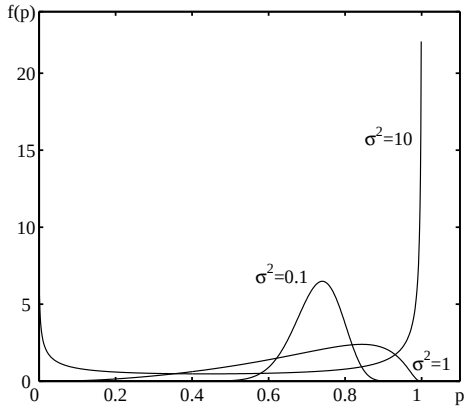

Figure 10: *The density of stationary open probability $P_s(p_\infty)$ due to voltage fluctuation with variance σ^2, at voltage potential $\Delta V = V_{1/2} - \langle V \rangle = 1$, and $c = 1$. Graphs illustrate effects of σ^2 = 0.1, 1, and 10. $\sigma^2 > 1$ results in a bimodal distribution that may produce hysteresis.*

4.3 Auto-regulation of voltage sensitivity

With mode transitions slower than voltage-dependent kinetics, we expect hysteretic effects of the kind observed for the NSVDC channel, voltage-independent conductance delays. To illustrate, figure 11 shows a dwell-time series from a single channel simulation of the four state channel, either starting in mode 1 (top) or mode 2 (bottom). It corresponds to priming a channel with either hyperpolarized or depolarized potentials, then stepping to one and the same potential, 0 mV. Both traces show shifts between modes, but also hysteretic effects, i.e. mode preference depending on initial condition.

In the HCN channel, mode transition rate is of the same order of magnitude as voltage-dependent gating. This makes it hard to separate modes in a dwell time record. With more pronounced differences in mode and voltage-dependent kinetics, single channel mode shifting is easier to identify and quantify. In real ion channels, however, we have no reason to expect only two modes. A Markov model with two modes works fairly well for the HCN channel, as long as it addresses coarse macroscopic data. In the case of the NSVDC channel, the dwell-time data suggests multiple modes, perhaps even graded ones.

The circular model easily accommodates multiple modes. The scheme (4.12) represents a circular model with five modes, with a central mode that represents the midpoint of activation at equilibrium, flanked by modes with increasing, symmetric shifts of activation. We adjust parameters according to the number of modes, but maintain the general structural properties of

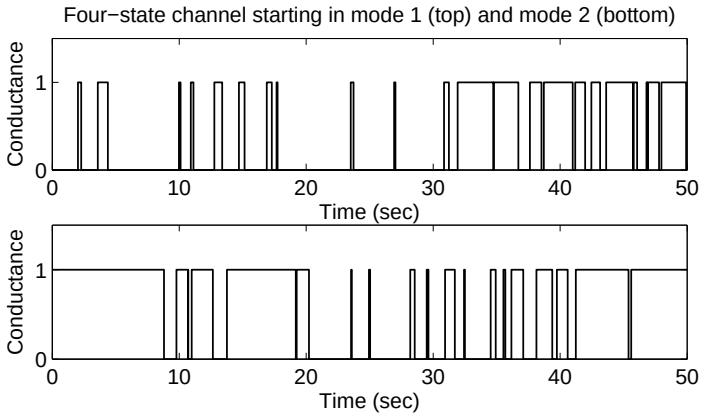

Figure 11: *Single channel hysteresis. The figure shows the results of a single channel simulation of the four-state circular model at 0 mV, with f=2.175 and* $\lambda = 0.1$*, starting in the closed state of mode 1 (top) and the open state of mode 2 (bottom) respectively.*

the four-state model.

$$\begin{array}{ccccccccc} [O_{i-k}] & ... & [O_{i-1}] & \underset{\frac{\lambda}{f}}{\overset{\lambda f}{\rightleftharpoons}} & [O_i] & \underset{\frac{\lambda}{f}}{\overset{\lambda f}{\rightleftharpoons}} & [O_{i+1}] & ... & [O_{i+k}] \\ \frac{\kappa_1}{f^{2k}} \upharpoonleft\downharpoonright \kappa_2 f^{2k} & & \frac{\kappa_1}{f^2} \upharpoonleft\downharpoonright \kappa_2 f^2 & & \kappa_1 \upharpoonleft\downharpoonright \kappa_2 & & \kappa_1 f^2 \upharpoonleft\downharpoonright \frac{\kappa_2}{f^2} & & \kappa_1 f^{2k} \upharpoonleft\downharpoonright \frac{\kappa_2}{f^{2k}} \\ [C_{i-k}] & ... & [C_{i-1}] & \underset{\lambda f}{\overset{\frac{\lambda}{f}}{\rightleftharpoons}} & [C_i] & \underset{\lambda f}{\overset{\frac{\lambda}{f}}{\rightleftharpoons}} & [C_{i+1}] & ... & [C_{i+k}] \end{array} \tag{4.12}$$

The scheme serves to illustrate a more general argument, that we expect increasing conductance delays with an increasing number of mode shifts. In figure 12, we show the simulation result of a circular model with eleven modes, with the same modeling principles as above. The allosteric factor is designed to produce the same maximum mode shift as in the four-state channel: f=1.1685 $\Rightarrow \Delta V \approx \pm 20$ mV at terminal end modes (k=5). As in the four-state case, the modes are traversed in a specific direction. In a closed state, the ion channel favors the mode with the highest midpoint of activation, resiting a transition to open state. The reverse holds for an open state, a preference for the mode with the lowest midpoint of activation, resiting a transition to closed state. The effect is an auto-regulation of conductance, i.e. *voltage-independent modulation of voltage-dependent kinetics.*

With an increasing number of modes, and with mode kinetics matching voltage-dependent kinetics, the mode shifting becomes less distinct, while the hysteretic effects get more pronounced. We are now closing in on the

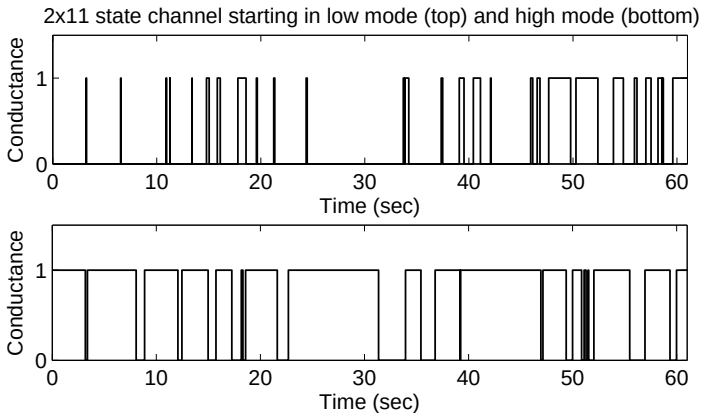

Figure 12: *Multiple mode hysteresis. The figure shows the results of a simulation of the 2x11-state model with 11 modes at 0 mV, with f=1.1685 and* $\lambda = 1$*, starting in the most probable closed state in low gating mode during hyperpolarization (top) and the most probable open state in high gating mode during depolarization (bottom).*

behavior of the NSVDC channel. With multiple modes and slower mode transition rates, the hysteretic effect can appear more or less continuous, more or less enduring. Single modes may become difficult to discern, blurring into each other, while the history-dependent voltage-dependent kinetics gets more and more pronounced. However, to generate truly continuous auto-regulated conductance, we may need to go beyond discrete Markov models. To model continuous auto-regulation, we must consider mechanisms like auto-catalysis and enzymatic mechanisms. For example, we can imagine active (open) ion channels generating a modulator [M] modifying the rate functions. The concentration of ion species is a natural candidate for a continuous modulator, but any chemical, electrical, and thermal effect of gating is a candidate. Such models need to be defined and evaluated in relation to particular ion channels.

5 Conclusions

Reports of ion channel hysteresis are rare, both at the macroscopic and the microscopic levels of observation. It does not mean that it is a rare property, or that it is without significance to ion channel function. It may as well be a result of research priorities. Traditional experimental protocols, generating relaxation records and dwell-time series, are standard methods that are often hard to reconcile with each other. On the one hand, relaxation records represent whole-cell conductances that are easier to model, whereas

dwell-time records reveal single ionic conductances. One the other hand, macroscopic records may be more true to ion channel activity in a more or less intact cell, whereas microscopic records of an isolated channel are more sensitive to experimental conditions, noise and perturbations.

Our argument here is hysteretic conductance provides alternative measures of voltage sensitivity, e.g. conductance loops. Even if much remains to be elaborated and formalized, we have shown that hysteretic conductance can serve to explore and evaluate the state space of voltage-dependent ion channels, e.g. independent versus cooperative gating. Hysteretic conductance is here a complement to traditional methods. Together with information on gating charge and conductance curves at equilibrium, independent and cooperative gating makes different predictions of hysteretic conductance. In principle, hysteretic conductance also allows us to test assumptions of independent gating schemes. More generally, it is a source of information on the voltage sensitivity of ion channels, providing indications of mode shifting, interactions between voltage-dependent and voltage-independent processes.

In living cells, there is constant interplay of electrodynamic and biochemical processes. Various molecular interactions modulate the voltage-dependency of ion channels. Mode-shifting is a specific case of "modal gating", a concept that also covers processes like inactivation and hyperactivation, sensitization and desensitization [13][17][20][31][48][51]. All are molecular processes that affect the voltage sensitivity of ion channels. Here we have only scratched the surface of the topic. In the future, we need to systematically compare various mechanisms that are involved in the regulation of the voltage-sensitivity of ion channels.

Another question that we leave unanswered is whether hysteretic conductance fulfils any real function in neural signaling. We have only discussed its value for modeling purposes. A couple of studies do indicate that hysteresis in HCN channels may in fact serve the regulation of oscillatory neural activity [1][12]. This is something that deserves more and careful attention in future research.

6 Acknowledgements

This work is supported by Swedish Foundation for Strategic Research and The Foundation of Helge Ax:son Johnson.

References

[1] Azene, E.M., Xue, T., Marbán, E., Tomaselli, G.F., and Li, R.A. Non-equilibrium behavior of HCN channels: Insights into the role of HCN channels in native and engineered pacemakers. Cardiovascular Research. 2005. 67:263-273.

[2] Baranauskas, G. Ionic Channel Function in Action Potential Generation: Current Perspective. Molecular Neurobiology (2007) 35:129-150.

[3] Baruscotti M, Bucchi A, and DiFrancesco. Physiology and pharmacology of the cardiac pacemaker ("funny") current. Pharmacology & Therapeutics. 2005. 107:59-79.

[4] Bennekou, P., Barksmann, T., Jensen, L.R., Kristensen, B.I., and Christophersen, P. Voltage activation and hysteresis of the non-selective voltage-dependent channel in the intact human red cell. Bioelectrochemistry 2004. 62:181-185.

[5] Bennekou, P., Kristensen, B.I., and Christophersen, P. The human red cell voltage-regulated cation channel. The interplay with the chloride conductance, the Ca^{2+}-activated K^+ channel and the Ca^{2+} pump. Journal of Membrane Biology. Septembre 2003. 195(1):1-8.

[6] Börjesson, S.I. and Elinder, F. Structure, Function, and Modification of the Voltage Sensor in Voltage-Gated Ion Channels. Cell Biochemistry and Biophysics. 52(3) 2008:149-74.

[7] Clarke, B.R. and McKinnon, P.K. Robust inference and modelling for the single ion channel. Journal of Statistical Computation and Simulation. Vol. 75, No. 7, July 2005:513-529.

[8] Colquhoun, D. and Hawkes, A.G. The Principles of the Stochastic Interpretation of Ion-Channel Mechanisms. In Single-Channel Recordings. Sackmann, B. and Neher, E. (Eds.) 1995. 2^{nd}Ed. New York, US: Plenmum Press.

[9] Colquhoun, D. and Hawkes, A.G. A Q-Matrix Cookbook: How to Write Only One Program to Calculate the Single-Channel and Macroscopic Predictions for Any Kinetic Mechanism. In Single-Channel Recordings. Sackmann, B. and Neher, E. (Eds.) 1995. 2^{nd}Ed. New York, US: Plenmum Press.

[10] Craven KB and Zagotta WN. CNG and HCN channels: two peas, one pod. Annual Review of Physiology. 2006. 68:375-401.

[11] Elinder F, Männikkö R, Pandey S, and Larsson HP. Mode shifts in the voltage gating of the mouse and human HCN2 and HCN4 channels. The Journal of Physiology. 2006. 575:417-31.

[12] Männikkö, R., Pandey, S., Larsson, PH., and Elinder, F. Hysteresis in the Voltage Dependence of HCN Channels: Conversion between Two Modes Affects Pacemaker Properties. The Journal of General Physiology. March 2005. 125:305-326.

[13] Fellin, T., Luvisetto, S., Spagnolo, M., and Pietrobon, D. Modal gating of human $Ca_V2.1$ (P/Q-type) calcium channels: II. the b mode and reversible uncoupling of inactivation. The Journal of General Physiology. November 2004. 124(5):463-74.

[14] Gudowska-Nowak E., Flyvbjerg H., Bennekou P. and Christophersen P. Hysteresis in Channel Gating. In Unsolved Problems of Noise and Fluctuations in Physics, Biology and High Technology. Bezrukov S. (ed.) American Institute of Physics Conference Proceedings. 2003. 665:305-311.

[15] Gurkiewicz, M. and Korngreen, A. A Numerical Approach to Ion Channel Modelling Using Whole-Cell Voltage-Clamp Recordings and a Genetic Algorithm. PloS Computational Biology. August 2007. Vol. 3(8):1633-47.

[16] Haliloglu T. and Ben-Tal N. Cooperative transition between open and closed conformations in potassium channels. PLoS Computational Biology. 2008;4(8):e1000164(1-11).

[17] Hille B. Ion Channels of Excitable Membranes. Sunderland, US: Sinauer Associates Inc, 2001 (3^{rd} edition).

[18] Hodgkin, A.L. and Huxley, A.F. A quantitative description of membrane current and its application to conduction and excitation in nerve. The Journal of Physiology. 1952. 117:500-544.

[19] Hosein-Sooklal, A and Kargol, A. Wavelet analysis of nonequilibrium ionic currents in human heart sodium channel (hH1a). Journal of Membrane Biology. 2002;188(3):199-212.

[20] Ionescu, L., White, C., Cheung, K.H., Shuai, J., Parker, I., Pearson, J.E., Foskett, J.K., Mak, D.O. Mode switching is the major mechanism of ligand regulation of $InsP_3$ receptor calcium release channels. The Journal of General Physiology. December 2007. 130(6):631-45.

[21] Jones, S.W. Are rate constants constant? The Journal of Physiology. 2006. 571(3):502.

[22] Kaestner, L., Christophersen, P., Bernhardt, I., and Bennekou, P. The non-selective voltage-activated cation channel in the human red blood cell membrane: reconciliation between two conflicting reports and further characterisation. Bioelectrochemistry 2000. 52:177-125.

[23] Kargol, A and Kabza, K. Test of the nonequilibrium kinetic focusing of voltage-gated ion channels. Physical Biology. 2008;5(2):26003.

[24] Kargol A and Hosein-Sooklal A. Optimal-sensitivity analysis of ion channel gating kinetics. Journal of Membrane Biology. 2004; 199(2):113-8.

[25] Kargol, A, Hosein-Sooklal, A, Constantin, L and Przestalski, M. Application of Oscillating Potentials to the Shaker Potassium Channel. In General Physiology and Biophysics. 2004; 23:53-75.

[26] Kargol, A, Smith, B and Millonas, M. Application of nonequilibrium response spectroscopy to the study of channel gating. Experimental design and optimization. Journal of Theoretical Biology. 2002; 218:239-258.

[27] Kock, C. Biophysics of Computation: Information Processing in Single Neurons. New York, US: Oxford University Press. 1999.

[28] Liebovitch, L.S., Scheurle, D., Rusek, M., Zochowski, M. Fractal methods to analyze ion channel kinetics. Methods. 2001. 24:359-375.

[29] Liebovitch, L.S., Fischbarg, J., and Koniarek, J.P. Ion Channel Kinetics: A Model Based on Fractcal Scaling Rather Than Multistate Markov Processes. Mathematical Biosciences. 1987. 84:37-68.

[30] Lin, W., Laitko, U., Juranka, P.F., and Morris, C. Dual Stretch Responses of mHCN2 Pacemaker Channels: Accelerated Activation, Accelerated Deactivation. Biophysical Journal. March 2007. Vol. 92:1559-1572.

[31] Luvisetto, S., Fellin, T., Spagnolo, M., Hivert, B., Brust, P.F., Harpold, M.M., Stauderman, K.A., Williams, M.E., and Pietrobon, D. Modal gating of human $Ca_V2.1$ (P/Q-type) calcium channels: I. The slow and the fast gating modes and their modulation by beta subunits. The Journal of General Physiology. November 2004. 124(5):445-61.

[32] McCormick, D.A., Shu, Y., and Yu, Y. Hodgkin and Huxley model — still standing? Nature. 445(4) January 2007.

[33] Majumdar, S. and Sikdar, S. Periodicity in Na^+ channel properties alters excitability of a model neuron. Biochemical and Biophysical Research Communications 359 (2007) 908-914.

[34] McManus, O.B,, Weiss, D.S., Spivak, C.E., Blatz, A.L., and Magleby, K.L. Fractal models are inadequate for the kinetics of four different ion channels. Biophysical Journal. 1988. 54:859-870.

[35] Menconi, M.C., Pellegrini, Mo., Pellegrino, Ma., and Petracchi, D. Periodic forcing of a single ion channel: dynamic aspects of the open-closed switching. The European Biophysical Journal. (1998)27:299-304.

[36] Michels G, Brandt MC, Zagidullin N, Khan IF, Larbig R, van Aaken S, Wippermann J, Hoppe UC. Direct evidence for calcium conductance of hyperpolarization-activated cyclic nucleotide-gated channels and human native If at physiological calcium concentrations. Cardiovascular Research. June 2008. 78(3):466-75.

[37] Milescu, L.S., Yamanishi, T., Ptak, K., Mogri, M.Z., and Smith, J.C. Real-Time Kinetic Modeling of Voltage-Gated Ion Channels Using Dynamic Clamp. Biophysical Journal. Volume 95. July 2008: 66-87.

[38] Millonas, M and Hanck, DA. Nonequilibrium response spectroscopy of voltage-sensitive ion channel gating. Biophysical Journal. 1998;74:210-229.

[39] Millonas, M and Hanck, DA. Nonequilibrium response spectroscopy and the molecular kinetics of proteins. Physical Review Letters. 1998;80:401-404.

[40] Millonas, MM and Chialvo, DR. Control of voltage-dependent biomolecules via nonequilibrium kinetic focusing. Physical Review Letters. 1996;76(3):550-553.

[41] Naundorf, B., Wolf, F., and Volgushev, M. Unique features of action potential initiation in cortical neurons. Nature. 440(20). April 2006.

[42] Nayak, T.K. and Sikdar, S.K. Time-dependent molecular memory in single voltage-gated sodium channel. Journal of Membrane Biology. October 2007, 219(1-3):19-36.

[43] Nekouzadeh, A. and Rudy, R. Statistical properties of ion channel records. Part I: Relationship to the macroscopic current. Mathematical Biosciences 210 (2007) 291-314.

[44] Nekouzadeh, A. and Rudy, R. Statistical properties of ion channel records. Part II: Estimation from the macroscopic current. Mathematical Biosciences 210 (2007) 315-334.

[45] Nowak L.M. and Wright, J.M. Slow Voltage-Dependent Changes in Channel Open-State Probability Underlie Hysteresis of NMDA Responses in Mg^{2+}-Free Solutions. Neuron, Vol. 8, 181-187, January, 1992.

[46] Ozer, M. A comparative analysis of linear, nonlinear and improved nonlinear thermodynamic models of voltage-dependent ion channel kinetics. Physica A. 2007. 379:579-586.

[47] Petracchi, D, Pellegrini, M, Pellegrino, M, Barbi, M and Moss, F. Periodic forcing of a K+ channel at various temperatures. Biophysical Journal. 1994;66(6):1844-52.

[48] Popescu, G. and Auerbach, A. Modal gating of NMDA receptors and the shape of their synaptic response. Nature Neuroscience. May 2003. Vol. 6(5):476-483.

[49] Pustovoit, M.A., Berezhkovskii, A.M., and Bezrukov, S.M. Analytical theory of hysteresis in ion channels: Two-state model. The Journal of Chemical Physics. 2006. 125(19):194907.

[50] Sansom, M.S., Ball, F.G., Kerry, C.J., McGee, R., Ramsey, R.L., and Usherwood, P.N. Markov, fractal, diffusion, and related models of ion channel gating. A comparison with experimental data from two ion channels. Biophysical Journal. December 1989. 56(6):1229-43.

[51] Schönherr, R., Mannuzzu, L.M., Isacoff, E.Y., and Heinemann, S.H. Conformational Switch between Slow and Fast Gating Modes: Allosteric Regulation of Voltage Sensor Mobility in the EAG K^+ Channel. Neuron. Vol.35, 935-949, August 29, 2002.

[52] Sigg D and Bezanilla F. Total charge movement per channel. The relation between gating charge displacement and the voltage sensitivity of activation. Journal of General Physiology. 1997;109(1):27-39.

[53] Uebachs, M., Schaub, C., Perez-Reyes, E., and Beck, H. T-type $Ca2^+$ channels encode prior neuronal activity as modulated recovery rates. The Journal of Physiology. 2006. 571(3):519-536.

[54] Villalba-Galea, C.A., Sandtner, W., Starace, D.M., and Bezanilla, F. S4-based voltage sensors have three major conformations. PNAS. 2008. 105(46):17600-7.

[55] Wahl-Schott, C. and Biel, M. HCN channels: Structure, cellular regulation and physiological function. Cell. Mol. Life Sci. 2008. Oct 27. Epub ahead of print.

[56] Yifrach O. Hill coefficient for estimating the magnitude of cooperativity in gating transitions of voltage-dependent ion channels. Biophysical Journal. 2004;87(2):822-30.

Statistical sensitivity analysis and remodeling of whole-cell conductances in nociceptors

Tom Andersson, Joanna Tyrcha, Olivia Eriksson

February 11, 2010

Stockholm University
Department of Mathematics
Section for Mathematical Statistics
toma@math.su.se
+46 70 594 43 23

Abstract

In whole-cell studies of neuronal excitability, modeling of neuronal conductance usually involves a large number of parameters that are often assumed to be constant, e.g. maximal conductance, midpoints and slopes of activation and inactivation. In neurons, the parameters do not correspond to static physiological correlates, but are subject to variation on different scales and levels. Here we show that statistical sensitivity analysis of parameter variations, and remodeling of systems of ordinary differential equations, can reveal clues to new mechanisms of neuronal firing, signal transduction pathways, other than the traditional mechanisms of stimulus and response. We take a closer look at a conduction model of nociceptors, i.e. primary sensory neurons involved in sensing noxious stimuli. The analysis involves four parts: (I) defining response measures, (II) optimal parameter sampling, (III) statistical sensitivity analysis, and (IV) ODE remodeling, i.e. translating statistical findings into mechanistic conductance components. The analysis ends up in experimental predictions: dual firing mechanisms, i.e. inactivation shifts of the TTX-resistent sodium current $Na_{TTX\text{-}R}$ and activation shifts of the delayed rectifier potassium current K_{DR}.

Key words: statistical sensitivity analysis, whole-cell conductance, nociceptor, systems biology, Hodgkin-Huxley, ODE system, dual coding, gain function

Contents

1 Introduction

The purpose of mathematical and computational modeling in systems biology is to explore the many and diverse signaling pathways that exist in living cells. Modeling and simulation allow for systematic manipulation of large numbers of components, often larger than the number of variables that can be controlled in a single experimental study. This enables us to explore cellular mechanisms that are hard or even impossible to measure experimentally, but it comes with a price. The more elaborate model, the more parameters enter into its making and the harder it gets to evaluate it, "the curse of dimensionality". Consequently, there is an increasing need for methods of model evaluation and sensitivity analysis. Here we present a statistical approach to sensitivity analysis of parameter variation in conductance models of neurons.

In conductance models of neurons, parameters are based on experimental research, but then often assumed constant. Still, the physiological correlates to the model parameters are subject to ubiquitous variation on different cellular levels and different spatiotemporal scales. When dealing with conductance models of neurons, we may discern at least three different kinds of parameter variation: (1) phenotypic variation between neurons (morphology), (2) electro- and biochemical regulation within neurons (expression and modulation of receptors and ion channels) and (3) random variation (ionic and molecular fluctuations). Variation of conductance model parameters exists at all three levels. In this article, our focus is on variation due to electro- and biochemical regulation within neurons, more specifically on variation of model parameters that may regulate the excitability of nociceptors.

Nociceptors refer to primary sensory neurons, i.e. dorsal root ganglion (DRG) C-type neurons, with high-thresholds,specifically involved in sensing harmful stimuli. The conductance properties of nociceptors are plastic and subject to regulation and modulation of diverse kinds (Amir et al 1999; Devor 1999; Matsutomi et al 2006; Okuse 2007; Rush et al 2007; Schmelz and Schmidt 2009; Smith and Lewin 2009; Belmonte and Viana 2009). They are polymodal, i.e. responding to both mechanical, thermal, and chemical stimuli. Recent findings also indicate that they also code for different stimuli, i.e. different response frequencies depending on the type of stimulus (Cavanaugh et al 2009; Olausson 1998). This raises a fundamental question regarding the coding properties of neurons. How do they separate and code for different stimuli when their output signal is regulated by one and the same compartment, a single axon? It is one thing that single neurons react to different stimuli. It is quite another thing that they code for different stimuli in their output (Koch 1999; Rieke et al 1999). This motivates a closer look at the conductance properties of nociceptors.

A characteristic feature of nociceptors is the presence of several types of sodium ion channels giving rise to multiple sodium conductances. So far

four sodium channels have been identified. Two of them drive the most well-known macroscopic currents: TTX-sensitive and TTX-resistant currents. These have been included in a published model that is the point of departure for our study, here called "the Herzog model" (Herzog et al 2001). The model relies on the classic Hodgkin-Huxley approach for modeling whole-cell conductance in single neurons (Hodgkin and Huxley 1952). The core assumption is that the cell membrane functions as a capacitor, in parallel with active (variable) and passive (fixed) resistors regulating different ionic currents, together making up a single circuit. It corresponds to the experimental condition of whole-cell measurement, i.e. measurements of whole-cell currents consisting of thousands of smaller microscopic currents through single ion channels. This modeling framework still guides experimental research on single neurons.

The aim here is to statistically analyze the excitability of the Herzog model to map the effects of parameter variations systematically. We increase the validity of the model by adding some well-known conductance components in nociceptors: a transient potassium current (Everill et al 1998) and a slow and a fast hyperpolarization-activated current (HCN, "queer currents") (Kouranova et al 2008; Momin et al 2008). With default values, the extended Herzog model reflects the response pattern of a class III neuron (Prescott et al 2008). When constant positive stimulus is applied, it fires once and then remains silent. It fires repeated action potentials in response to negative stimulation, but does not manifest any monotone response function of stimulus intensity. By exploring the model excitability in relation to random parameter variations, we hope to discover alternative mechanisms of spiking.

Within systems biology, studies of parameter variability are often referred to as exploring the robustness or fragility of the networks. When a large range of parameter values supports the same dynamical behavior, the system is considered robust (Marino et al 2008; Stelling et al 2004). Here we hypothesize that sensitive parameters can also be sensitive for a reason, not only being an annoyance, but allowing for regulation and modulation of system output (Ingalls 2008; Saltelli et al 2000). By identifying critical and modulatory parameters in experimental models, we generate hypotheses regarding transduction and conduction mechanisms, i.e. mechanisms involving biochemical and electrochemical regulation of neuronal excitability. To our knowledge, this method of exploring potential regulatory and modulatory parameters by statistical sensitivity analysis has not been done before, even if there are related approaches (Weaver and Wearne 2008).

The study involves four steps: (1) defining response measures, (2) developing and testing sampling protocols, (3) statistical sensitivity analysis of response functions, and (4) remodeling of conductance components. As systems of ordinary differential equations (ODE), conductance models do not separate non-firing and firing responses. Therefore the first step is to

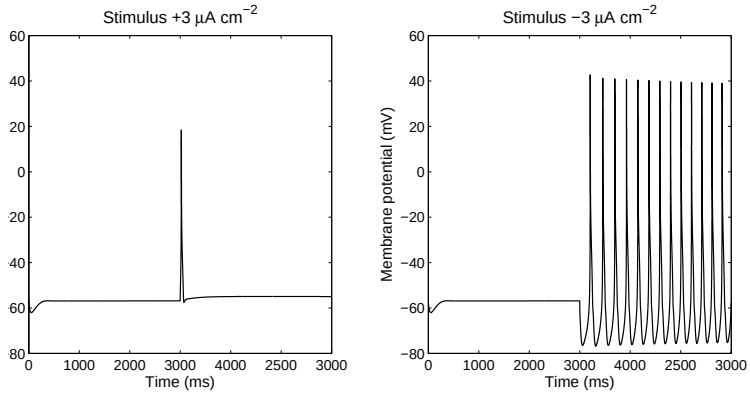

Figure 1: Firing behavior of the Herzog model in response to positive and negative stimulation applied after 3000 ms run time.

define relevant response measures, i.e. *measures of system activity based on time series of system variables*. After this, we identify an optimal sample of parameter variation, i.e. a sample generating maximal correlation between input and output, allowing for sampling without pre-defined ranges of parameter values. This sample is the basis for further statistical sensitivity analysis of response functions, i.e. *effects of random parameter variation on response measures*. We make use of logistic and linear regression analysis (Davison 2003; Dobson and Barnett 2008) to identify critical and modulatory parameters of excitability.

The final step is the remodeling of statistical response functions into realistic conductance mechanisms. The parameter sampling is based on the unrealistic assumption of normal distribution of parameter values. Therefore, we need to translate the statistical findings into plausible conductance mechanisms. This is done by remodeling some of the conductance components in the original model, thereby validating the statistical findings. The conclusion is that our model allows for alternative mechanisms of excitability. Different parameters of the delayed K current and the TTX-resistant Na^+ current respectively support different ranges of frequency responses, in principle allowing for regulation and modulation of system output by different signal transduction pathways.

2 An extended conductance model of nociceptors

The Herzog model is a single compartment model of a primary sensory DRG neuron. In its basic form, it includes two sodium (Na^+) currents, TTX-S and TTX-R, one delayed rectifier potassium (K^+) current, and one leakage current. The sodium conductances are regulated by both activation

Parameter	Value	Description
C	0.81 μF cm^{-2}	Capacitance
E_{Na}	62.94 mV	Reversal potential for Na^+-current
E_K	-92.34 mV	Reversal potential for K^+-current
E_Q	-30 mV	Reversal potential for Q-current
E_L	-54.3 mV	Reversal potential for leak current
$\overline{g}_{Na_{TTX-S}}$	35.1 mS cm^{-2}	Maximum conductance for Na_{TTX-S}
$\overline{g}_{Na_{TTX-R}}$	6.9 mS cm^{-2}	Maximum conductance for Na_{TTX-R}
$\overline{g}_{Kdr}$	2.1 mS cm^{-2}	Maximum conductance for Kdr
$\overline{g}_{Ka}$	1.05 mS cm^{-2}	Maximum conductance for Ka
$\overline{g}_{Q_{fast}}$	0.15 mS cm^{-2}	Maximum conductance for Q_{fast}
$\overline{g}_{Q_{slow}}$	0.15 mS cm^{-2}	Maximum conductance for Q_{slow}
$\overline{g}_{Leak}$	0.14 mS cm^{-2}	Constant conductance for leak current
I_{stim}	0 mV	Zero defines default resting potential V_i
V_i	-59 mV	Initial membrane potential (default: 59 mV)

Table 1: Default parameter values in the main voltage equation in the extended Herzog model

and inactivation, whereas the slow potassium conductance is regulated by activation alone. To this core model, we have added three currents, one fast transient K^+ current, one fast and one slow hyperpolarization-activated (Q) currents. The fast K^+ current has been added to agree with general research findings on DRG neurons. The delayed K^+ current is dominant, but a smaller fast transient K^+ current is also observed (Everill 1998). The equations for the K^+ current has been taken from a more elaborate model of a nodose neuron, which actually inspired the Herzog model in the first place (Schild et al 1997). The two Q currents have been defined in an article on the expression and distribution of HCN channels, where the authors also included the currents in the Herzog model to study their effects on single spike kinetics (Kouranova et al 2008). We reuse formulas and parameter values also in this case.

The extended Herzog model consists of ten differential equations, one main voltage equation and nine gating functions. The main equation (2.1) defines voltage kinetics, i.e. change of membrane potential as a function of ionic currents. The gating functions (2.2-2.10) specify ion channel kinetics, i.e. ionic conductance changes as a function of voltage dependence. Table 1 lists default parameter values of the main voltage equation. Table 2 summarizes the nine gating functions. Table 3 specifies default parameter values in the gating functions (equations 2.2-2.10). The parameters are not explicitly represented by names, but by their values.

Variables	Description
V	Voltage (membrane potential)
m_1	Activation of Na $_{\mathrm{TTX-S}}$ conductance
m_2	Activation of $Na_{\mathrm{TTX-R}}$ conductance
n_1	Activation of Kdr conductance
n_2	Activation of Ka conductance
h_1	Inactivation of $Na_{\mathrm{TTX-S}}$ conductance
h_2	Inactivation of $Na_{\mathrm{TTX-R}}$ conductance
h_3	Inactivation of Ka conductance
q_1	Activation of fast Q conductance
q_2	Activation of slow Q conductance

Table 2: Variables (functions) in the extended Herzog model

$$
\begin{aligned}
C\frac{dV}{dt} &= -(I_{Na_{TTX-S}} + I_{Na_{TTX-R}} + I_{Kdr} + I_{Ka} \\
&\quad + I_{q-fast} + I_{q-slow} + I_{leak} - I_{stim}) \qquad (2.1)\\
I_{Na_{TTX-S}} &= \overline{g}_{Na_{TTX-S}} m_1^3 h_1 (V - E_{Na}) \\
I_{Na_{TTX-R}} &= \overline{g}_{Na_{TTX-R}} m_2 h_2 (V - E_{Na}) \\
I_{kdr} &= \overline{g}_{Kdr} n_1 (V - E_K) \\
I_{ka} &= \overline{g}_{Ka} n_2^3 h_3 (V - E_K) \\
I_{q-fast} &= \overline{g}_{Q-fast} q_1 (V - E_Q) \\
I_{q-slow} &= \overline{g}_{Q-slow} q_2 (V - E_Q) \\
I_{leak} &= \overline{g}_{leak} (V - E_L) \\
I_{stim} &= external\ current\ (\mu A\ cm^{-2})
\end{aligned}
$$

$$
\begin{aligned}
\frac{dm_1}{dt} &= \frac{m_1(\infty) - m_1}{\tau_{m_1}} \qquad (2.2)\\
m_1(\infty) &= \frac{\alpha_{m_1}}{\alpha_{m_1} + \beta_{m_1}} \\
\tau_{m_1} &= \frac{1}{\alpha_{m_1} + \beta_{m_1}} \\
\alpha_{m_1} &= \frac{11.49}{1 + e^{\frac{V+8.58}{-8.47}}} \\
\beta_{m_1} &= \frac{11.49}{1 + e^{\frac{V+67.2}{27.8}}}
\end{aligned}
$$

Parameter	Value	Description
U_{m_1}	-21.6 mV	Voltage midpoint of activation for Na_{TTX-S}
U_{m_2}	-40 mV	Voltage midpoint of activation for Na_{TTX-R}
U_{n_1}	-14.6 mV	Voltage midpoint of activation for Kdr
U_{n_2}	-28 mV	Voltage midpoint of activation for Ka
U_{q_1}	-87.2 mV	Voltage midpoint of activation for Q_{fast}
U_{q_2}	-87.2 mV	Voltage midpoint of activation for Q_{slow}
U_{h_1}	-72.9 mV	Voltage midpoint of inactivation for Na_{TTX-S}
U_{h_2}	-57 mV	Voltage midpoint of inactivation for Na_{TTX-R}
U_{h_3}	-58 mV	Voltage midpoint of inactivation for Ka
k_{m_1}	8.5	Slope of activation for Na_{TTX-S}
k_{m_2}	9.9	Slope of activation for Na_{TTX-R}
k_{n_1}	18	Slope of activation for Kdr
k_{n_2}	28	Slope of activation for Ka
k_{q_1}	9.7	Slope of activation for Q_{fast}
k_{q_2}	9.7	Slope of activation for Q_{slow}
k_{h_1}	7.9 mV	Slope of inactivation for Na_{TTX-S}
k_{h_2}	3.1 mV	Slope of inactivation for Na_{TTX-R}
k_{h_3}	7 mV	Slope of inactivation for Ka

Table 3: Gating parameters and their default values in the extended Herzog model

$$\begin{aligned} \frac{dm_2}{dt} &= \frac{m_2(\infty) - m_2}{\tau_{m_2}} \\ m_2(\infty) &= \frac{\alpha_{m_2}}{\alpha_{m_2} + \beta_{m_2}} \\ \tau_{m_2} &= \frac{1}{\alpha_{m_2} + \beta_{m_2}} \\ \alpha_{m_2} &= \frac{1.032}{1 + e^{\frac{V+6.99}{-14.87115}}} \\ \beta_{m_2} &= \frac{5.79}{1 + e^{\frac{V+130.4}{22.9}}} \end{aligned} \tag{2.3}$$

$$\begin{aligned}
\frac{dn_1}{dt} &= \frac{n_1(\infty) - n_1}{\tau_{n_1}} \\
n_1(\infty) &= \frac{1}{1 + e^{\frac{V+14.62}{-18.38}}} \\
\tau_{n_1} &= \frac{1}{\alpha_{n_1} + \beta_{n_1}} \\
\alpha_{n_1} &= \frac{0.001265(V + 14.273)}{1 - e^{\frac{V+14.273}{-10}}} \\
\beta_{n_1} &= 0.125\frac{(V + 55)}{-2.5}
\end{aligned} \tag{2.4}$$

$$\begin{aligned}
\frac{dn_2}{dt} &= \frac{n_2(\infty) - n_2}{\tau_{n_2}} \\
n_2(\infty) &= \frac{1}{1 + e^{\frac{V+28}{-28}}} \\
\tau_{n_2} &= 5e^{-0.022^2(V+65)^2} + 2.5
\end{aligned} \tag{2.5}$$

$$\begin{aligned}
\frac{dh_1}{dt} &= \frac{h_1(\infty) - h_1}{\tau_{h_1}} \\
h_1(\infty) &= \frac{\alpha_{h_1}}{\alpha_{h_1} + \beta_{h_1}} \\
\tau_{h_1} &= \frac{1}{\alpha_{h_1} + \beta_{h_1}} \\
\alpha_{h_1} &= 0.0658e^{\frac{-(V+120)}{20.33}} \\
\beta_{h_1} &= \frac{3}{1 + e^{\frac{V-6.8}{-12.998}}}
\end{aligned} \tag{2.6}$$

$$\begin{aligned}
\frac{dh_2}{dt} &= \frac{h_2(\infty) - h_2}{\tau_{h_2}} \\
h_2(\infty) &= \frac{\alpha_{h_2}}{\alpha_{h_2} + \beta_{h_2}} \\
\tau_{h_2} &= \frac{2}{\alpha_{h_2} + \beta_{h_2}} \\
\alpha_{h_2} &= \frac{0.06435}{1 + e^{\frac{V+73.26415)}{3.71928}}} \\
\beta_{h_2} &= \frac{0.13496}{1 + e^{\frac{V+10.27853}{-9.09334}}}
\end{aligned} \tag{2.7}$$

$$\begin{aligned} \frac{dh_3}{dt} &= \frac{h_3(\infty) - h_3}{\tau_{h_3}} \\ h_3(\infty) &= \frac{1}{1 + e^{\frac{V+58}{7}}} \\ \tau_{h_3} &= 100e^{-0.035^2(V+30)^2} + 10.5 \end{aligned} \tag{2.8}$$

$$\begin{aligned} \frac{dq_1}{dt} &= \frac{q_1(\infty) - q_1}{\tau_{q_1}} \\ q_1(\infty) &= \frac{1}{1 + e^{\frac{V+87.2}{9.7}}} \\ \tau_{q_1} &= \begin{cases} 250 + 12e^{\frac{V+240}{50}} & \text{if } V < -70 \\ 140 + 50e^{\frac{V+25}{-20}} & \text{if } V \geq -70 \end{cases} \end{aligned} \tag{2.9}$$

$$\begin{aligned} \frac{dq_2}{dt} &= \frac{q_2(\infty) - q_1}{\tau_{q_2}} \\ q_2(\infty) &= \frac{1}{1 + e^{\frac{V+87.2}{9.7}}} \\ \tau_{q_2} &= \begin{cases} 2500 + 100e^{\frac{V+240}{50}} & \text{if } V < -70 \\ 300 + 542e^{\frac{V+25}{-20}} & \text{if } V \geq -70 \end{cases} \end{aligned} \tag{2.10}$$

3 Response measures and sampling protocols

The extended Herzog model consists of 32 parameters (table 1 and 3 above). To record and analyze the effects of parameter variation on model output, we run computer simulations of the model with all parameters treated as independent random variables. A simulation results in a time series of data, i.e. a time sequence of voltage potentials, given a set of random parameters. The time series constitutes a single observation in a larger sample of time series for statistical analysis.

We use Matlab's ODE45 to solve the ODE system, with 2 seconds of run time and a time step of 1 μs. The first second serves the purpose of letting the system adjust to the parameter setup, to reduce excessive effects of initially unstable system conditions. After initial calibration, we record voltage potentials during a second. The time window of one second is a compromise between three competing goals: fast simulation run time, stable system conditions and agreement with experimental protocols in electrophysiological research.

3.1 Defining response measures

The Herzog model is a single electrical circuit. Stimulus I_{stim} is the input. Voltage $V(t)$ is the output. In itself, it lacks criteria for deciding what is to be counted as effective neuronal responses (firing). Mathematically, we can analyze the asymptotic behavior of the ODE system and define different attractors, such as states of equilibrium and stable oscillation. However, neuronal firing is something more and less than that. On the one hand, it is not restricted to oscillations of membrane potentials. Firing may refer to transient spikes or single spikes. On the other hand, not all neuronal oscillations constitute firing, e.g. subthreshold oscillations, oscillations of low amplitude. Firing refers to spikes of critical amplitude, although we lack criteria for deciding on the critical levels.

To analyze firing dynamics on the basis of time series of voltage potentials, we need response measures that account for both discrete and continuous properties of system output, i.e. transitions between discrete states of non-firing and firing, denoted $\eta \in \aleph$, as well as monotone change in frequency and amplitude of periodic responses, ω and $\theta \in \Re^+$. To this end, we define five response measures based on the time series of voltage output: (1) maximum autocorrelation coefficient ρ, (2) standard deviation σ, (3) class $\eta = \{1, 2, 3\}$, (4) dominant frequency ω for class $\eta = \{2, 3\}$, and (5) dominant amplitude θ for class $\eta = \{2, 3\}$. We define each response measure in turn. We begin with the maximum autocorrelation coefficient, namely

$$\rho_{n,m} = max\left(\rho_{n,m,\tau}\right) \text{ for } \tau > \tau_{min(\rho_{n,m,\tau})} \tag{3.1}$$

where

$$\rho_{n,m,\tau} = \frac{\sum_{i=1}^{N-\tau}\left(V(t_i) - \frac{\sum_{j=1}^{N} V(t_j)}{N}\right)\left(V(t_i+\tau) - \frac{\sum_{j=1}^{N} V(t_j)}{N}\right)}{\sum_{i=1}^{N}\left(V(t_i) - \frac{\sum_{j=1}^{N} V(t_j)}{N}\right)^2}, \tag{3.2}$$

where τ is a time lag, (n,m) represents the simulation run (n=$\{1,2,...,5000\}$) and the sample (m=$\{1,2,3\}$).

The maximum autocorrelation coefficient is a measure of the quality of periodic response, $0 < \rho < 1$. To exclude autocorrelation coefficients at lag zero, unity, ρ is here defined as the maximum coefficient at time lags greater than the time lag of the minimum autocorrelation coefficient.

The autocorrelation coefficient is a relatively straightforward measure of periodic responses. It is more difficult to define a measure of amplitude that take the potential diversity of spike forms into account. A basic measure is σ, the standard deviation of the time series of voltage potentials:

$$\sigma_{n,m} = \sqrt{\frac{1}{N}\sum_{i=1}^{N}\left(V\left(t_i\right) - \frac{\sum_{j=1}^{N} V\left(t_j\right)}{N}\right)^2} \tag{3.3}$$

The standard deviation cannot account for irregular spike forms, for example a short versus a long single spike. In such a case, the maximum may be the same, but σ differs due to the averaging of voltage potentials over the time series. Despite the shortcomings, the standard deviation is our basic measure of amplitude.

K-means cluster analysis is a method of data analysis and classification. To account for discrete transitions between non-firing and firing responses, we apply k-means cluster analysis to the simulation runs based on the autocorrelation coefficient ρ and the standard deviation σ, using the shortest Euclidean distance after standardization of variables.

The observations are clustered into three classes η={1,2,3}. We choose three classes (3-means cluster analysis) to make it easier to discover potential competing mechanisms generating borderline weak responses: (1) resting potentials ($\sigma \approx 0$, $\rho \approx 0$), (2) weak responses ($\sigma > 0$ and $\rho > 0$) and (3) proper firing ($\sigma \gg 0$ and $\rho \gg 0$). To evaluate the cluster analysis, we calculate pair-wise rank correlations between η and the other response measures, choosing a clustering that generates maximum correlation.

For proper firing responses $\eta = 3$, we apply two further response measures: dominant frequency ω and dominant amplitude θ. The dominant frequency ω, defined as

$$\omega_{n,m} = \frac{1}{\tau_{\rho_{n,m}}}, \tag{3.4}$$

is the frequency corresponding to $\rho_{n,m}$, the maximum autocorrelation coefficient. There may be more than one response frequency in time series of voltage potentials, but to simplify, we leave this out of account.

Maximum voltage minus minimum voltage θ is another measure of spike amplitude:

$$\theta_{n,m} = Max(V(t_i)) - Min(V(t_j)) \text{ for all } \{i,j\} \in \{1,...,N\} \tag{3.5}$$

In contrast to σ, an average, θ is based on two single values in the voltage time series. This makes it sensitive to non-stationary simulations, e.g. steady increases or decreases of voltage potentials. When limited to known periodic responses $\eta = 3$, its sensitivity is an advantage, enabling estimation of the amplitude of both regular and irregular forms of spiking.

Our response measures (ρ, σ, η, ω and θ) constitute a first attempt to define measures for statistical sensitivity analysis of neuronal models. They have limitations. For example, they cannot account for single spikes. Single

	Source of variation	
Parameter class	Within neurons	Across neurons
Stimuli	High	High
In-/activation midpoints	Moderate	High
Slope of in-/activation	Moderate	High
Maximum conductance	Moderate	High
Reversal potentials	Low	Moderate
Capacitance	Low	Moderate

Table 4: Parameter classes correspond neuronal properties subject to temporal and structural variation due to varying electro- and biochemical conditions, structural and morphological differentiation (within or across neurons). The type and magnitude of variation depends on parameter class. For example, stimuli are of diverse kinds and vary greatly in both space and time. In contrast, reversal potentials are comparatively stable for a single cell, even if they do very between cells and tissues. The table is based on the authors subjective summary of diverse research findings.

spikes are not periodic, implying zero/small autocorrelation coefficients ρ making them equal to resting states of neurons. Still, it is in agreement with the most basic measure of neuronal responses, i.e. spike frequency. Since single spikes occur once over an infinite period, they have zero frequency and constitute non-responses.

3.2 Sampling of model parameters

The extended Herzog model includes 32 parameters. To study and analyze response effects of parameter variation, we treat parameters as random variables with model default values as expected values. We sample parameter values from normal distributions. To define the variance of the sampling distributions, we consult experimental findings. However, it is not possible to make equally informed decisions on every single parameter. Furthermore, estimates are seldom comparable across experimental studies. Therefore, the strategy is to apply a common format of variation to six classes of the model parameters.

In table 4, we list sex parameter classes together with subjective judgements of relative levels of variation. Stimuli demonstrate high temporal and structural variation, i.e. numerous transient synaptic stimuli and diverse transduction processes. Other parameters that demonstrate high or moderate variation indicate alternative mechanisms of neuronal stimulation than direct postsynaptic depolarization. Parameters that demonstrate less variation, e.g. reversal potentials and capacitance, are less likely to function as regulators or modulators of neuronal firing.

Since the purpose of this study is to uncover alternative mechanisms of

	Magnitude		
Sampling protocol	**Small**	**Medium**	**Large**
Stimuli	N(0,1)	N(0,2.5)	N(0,5)
In-/activation midpoints	N(0,2.5)	N(0,5)	N(0,10)
Slope of in-/activation	N(0,2.5*)	N(0,5*)	N(0,10*)
Maximum conductance	N(0,5*)	N(0,10*)	N(0,15*)
Capacitance	N(0,2.5*)	N(0,5*)	N(0,10*)
Reversal potentials	N(0,0.5)	N(0,1)	N(0,2.5)

Table 5: Sampling protocol for model parameters. Random sampling of parameter values is made from normal distributions. The distributions in the table specify distributions of deviations from mean values, the default values of model parameters (table 1 and 3). "*" marks a standard deviation that is rendered in % of default value of model parameter. There is one exception to the sampling protocol: the midpoints of activation for the h-conductances $g_{Q_{slow}}$ and $g_{Q_{fast}}$ (see main text).

firing dynamics according to an existing model, and in a particular type of neuron, i.e. nociceptors, the overall sampling of parameter variations must be conservative. The parameter variations should reflect temporal variation due to biochemical modulation of conductances within single neurons, not structural variation across neurons. This means that our focus is on the variation in voltage midpoints of activation and inactivation, as well as slopes of activation and inactivation. We also allow for moderate variation of maximal conductance within single neurons.

Because different units and scales apply to the model parameters, it is not advisable to apply a single consistent rule of parameter variation, e.g. 1 % of default values. To illustrate why, current is a quantity measured on a ratio scale. It takes positive as well as negative values. In contrast, the midpoint of activation is a positional measure. It is the membrane voltage at which a conductance component is at 50% of its maximal activity, a measure of electrochemical activity that does not allow for relative measures (%).

Table 5 summarizes our sampling protocol, i.e. the sampling distributions for the six parameter classes. Due to the uncertainty in the range of parameter values, we define and test three levels of parameter variation: small, medium and large parameter variation. Medium variation corresponds to the level of variation that we judge to be reasonable for generating shifts in firing dynamics of neuronal conductance models, i.e. transitions between firing and non-firing. The large and small levels of variation are relative to the medium level, about 50% and 200% of the medium level.

There is one exception to the sampling protocol: the voltage midpoint of the Q-conductances: $g_{Q_{slow}}$ and $g_{Q_{fast}}$. Under default parameter values, the conductance is more or less inactive in the Herzog model. To have any

effect on firing dynamics, the activation midpoints must be shifted towards depolarized potentials. Therefore, we add a Bernoulli-distributed random indicator function $\delta \sim$ Bernoulli(0.5), specifying a shift of +20 mV or not, corresponding to reported shifts of Q-conductances (Kouranova et al 2008). Irrespectively of this shift, the activation midpoints are also subject to normal variation around their default or shifted values.

The sampling protocol also needs to be elaborated for another non-specified parameter: the initial voltage potential V_i. In computer simulations, V_i is usually set to the resting membrane potential (−70 mV), or the reversal potential of the leakage current. In this study, since we vary the parameter setup at random, we also randomize V_i. Since V_i is a measure of equilibrium, like voltage midpoints of activation, we give the same parameter distribution to V_i as to midpoints of in-/activation.

3.3 Optimal sample size and parameter variation

To evaluate which level of parameter variation (small, medium, large) that provides maximal information on response effects, computer simulations are run with three samples from the specified distributions above. The samples are compared with respect to the strength of the linear relationships that they generate between response measures and parameters. The strength is measured by the bivariate rank correlations $r_{i,j}$ between response measures ψ, $\psi \in \{\rho, \sigma, \eta\}$, and by the generalized sample rank correlation $|R_\psi|$ (cf. "generalized sample variance of the standardized variables" in Johnson and Wichern 2007), i.e. the determinant of the sample rank correlation matrix (size: 33 x 33) of all 32 parameters and a response variable ψ:

$$|R| = \left| \begin{bmatrix} r_{1,1} & r_{1,2} & \dots & r_{1,33} \\ r_{2,1} & r_{2,2} & \dots & r_{2,33} \\ \vdots & \vdots & \ddots & \vdots \\ r_{33,1} & r_{33,2} & \dots & r_{33,33} \end{bmatrix} \right| \tag{3.6}$$

where $r_{i,j}$, i and j $\in$ 1,...,33, is the Spearman rank correlation between variable i and j; variables 1-32 being the set of 32 independent random model parameters, variable 33 referring to ψ, one of the five response variables. When $r_{i,j} = 0$ for i≠j, $|R_\psi| = 1$. Any linear dependence between variables results in a reduction of $|R_\psi|$. Since random sampling of model parameters is independent, any significant reduction of $|R_\psi|$ is due to dependencies between some model parameter(s) and the response variable in question.

Maximal reduction of $|R_\psi|$, i.e. min($|R_\psi|$), defines the optimal sample: maximal dependency of the response measure on model parameters. This presupposes that the correlation between parameters is non-existent or low. With a large number of parameters, and a small number of observations, random correlations multiply and result in large reductions of $|R_\psi|$. To

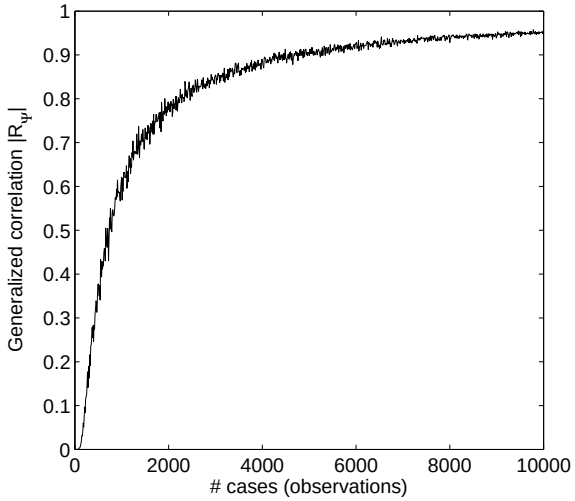

Figure 2: A plot of generalized correlation $|R_\psi|$ for 32 independent random variables (N(0,1)) as a function of sample size. Below 2500 cases, normally distributed drops and increases in uncertainty.

# cases	Small	Medium	Large
$\eta = 1$	4110	3541	3597
$\eta = 2$	288	413	754
$\eta = 3$	602	1046	649

Table 6: Cross-tabulation of the number of responses with respect to level of variation and response cluster

decide on sufficient sample size to secure high and stable $|R_\psi|$, we simulated 32 independent random parameters for varying sample sizes. A sample size of 5000 results in $|R_\psi|$ high and stable enough for our purposes (figure 2).

After establishing the sample size, we put three samples to test (small, medium and large levels of parameter variation). The purpose is to identify the sample that gives us maximum information on relations between parameter variation and response measures. Each sample consists of N=5000 cases of 32 independent random parameter values. Computer simulations generate 3 x 5000 time series of voltage potentials, summarized by $\rho_{n,m}$ and $\sigma_{n,m}$. 3-means cluster analysis based on ρ and σ results in three response classes: $(\eta = 1)$ resting, $(\eta = 2)$ weak responses and $(\eta = 3)$ firing. An optimal sample is one with large and balanced numbers of responses in $\eta = 1$ and $\eta = 3$, and as few as possible in $\eta = 2$.

The number of responses in $\eta = 3$ is highest for medium variation. The number of positive responses ($\eta \in \{2, 3\}$ is smaller for the sample with small

Matrix/Sample	Small	Medium	Large
$\|R_\sigma\|$	0.5085	0.4467	0.6425
$\|R_\rho\|$	0.4748	0.4412	0.6622
$\|R_\eta\|$	0.4950	0.4563	0.6565

Table 7: Generalized sample correlation $|R_\psi|$

Rank correlation/Variation	Small	Medium	Large
ρ and σ	0.3956	0.6249	0.6146
ρ and η	0.6633	0.7858	0.7681
σ and η	0.6405	0.7777	0.7679

Table 8: Spearman's rank correlations between pair-wise response measures for three samples with small, medium and large levels of parameter variation

parameter variation (table 6). The number of weak responses is larger for the sample with large variation. This indicates that medium variation is the more optimal sample. $|R_\psi|$ confirms this. A sample with 32 random parameters and 5000 cases makes $|R| \approx 0.90$ (figure 2). When including response variables one at the time, the reduction of $|R_\psi|$ is maximal for medium variation (table 7). Pair-wise rank correlations between response variables lend further support to this. In table 8, we list the correlations. The sample with medium parameter variation has the highest pair-wise rank correlations.

In figure 3, we render the clustering of the medium sample: ρ with respect to σ. The clustering is the basis for further statistical analysis in the next section, i.e. regression models of parameters on η (logistic regression), on ω (linear regression), and on θ (linear regression).

4 Statistical sensitivity analysis

The aim of statistical sensitivity analysis is to identify and compare sources of variation in firing responses, i.e. specifying relative merits of parameters for neuronal excitability and firing dynamics. The analysis involves three parts: (I) logistic regression of model parameters on non-firing and firing states ($\eta \in \{1, 2, 3\}$), and linear regression of model parameters on (II) dominant frequency ω and (III) dominant amplitude θ respectively.

4.1 Regulators of firing responses

To estimate the influence of model parameters on the probability of a firing response, we carry out multinomial logistic regression analysis of response cluster $\eta = \{1, 2, 3\}$ on standardized scores of model parameters (mean 0 and standard deviation 1). The response η is then modeled in terms of the

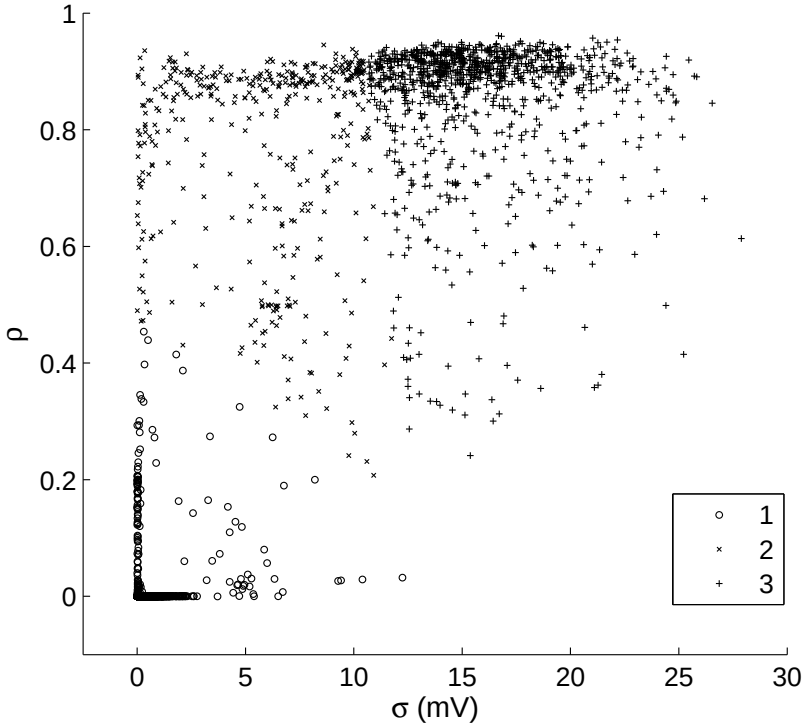

Figure 3: Mapping of response clusters for the sample with moderate level of parameter variation on a plot of response measures: ρ with respect to σ. The numbers of responses in cluster 1, 2 and 3 are 3541, 413 and 1046 respectively.

probability of outcomes $p(\eta)$, which are estimated by maximum likelihood ($max(L(\pi))$ (Dobson and Barnett 2008).

$$
\begin{aligned}
p(\eta) &= \binom{1}{\eta_1, \eta_2, \eta_3} \pi_1^{\eta_1} \pi_2^{\eta_2} \pi_3^{\eta_3} && (4.1)\\
&= \pi_1^{\eta_1} \pi_2^{\eta_2} \pi_3^{\eta_3}, && (4.2)\\
&\quad \sum_{i=1}^{3} \eta_i = 1,\ \eta_i \in \{0,1\}, \\
&\quad \sum_{i=1}^{3} \pi_i = 1,\ \pi_i \in [0,1] \\
log\left(\frac{\pi_{\{2,3\}}}{\pi_1}\right) &= \alpha_{\{2,3\}} + \beta_{1,\{2,3\}} * x_{n,1} + \ldots && (4.3)\\
&\quad \ldots + \beta_{k,\{2,3\}} * x_{n,k} \\
&\quad n \in \{1...5000\} \\
&\quad k \in \{1...32\} \\
L(\pi(\alpha,\beta)) &= \prod_{n=1}^{5000} \pi_1(\alpha,\beta)^{\eta_{1,n}} \pi_2(\alpha,\beta)^{\eta_{2,n}} \pi_3(\alpha,\beta)^{\eta_{3,n}} && (4.4)
\end{aligned}
$$

The probability of non-firing π_1 is the standard of comparison, in relation to which we evaluate the probability of weak responses π_2 and proper firing π_3 respectively. This is done by modeling the odds for active responses: $\frac{\pi_2}{\pi_1}$ and $\frac{\pi_3}{\pi_1}$. The first step is to analyze the effects of model parameters on these odds one at the time (OAT). The result is a highly limited number of parameters making any difference.

Table 9 lists model parameters with deviances greater than 10. Deviance is a measure of model fit, a comparison of log likelihoods. In this case, we compare log likelihoods of logistic models including a model parameter or the intercept-only. A larger deviance, i.e. a larger deviance reduction compared to the intercept-only model, makes the better fit. One parameter stands out from the rest, $\mathrm{U_{h_2}}$, the voltage midpoint of inactivation for $\mathrm{Na_{TTX-R}}$. It reduces the deviance of the intercept only model by 28.4 % (McFadden's pseudo-R-square). Two further parameters have a clear impact: stimulus S and $\mathrm{U_{n_1}}$, the activation midpoint of $\mathrm{K_{DR}}$. Additional eight parameters make smaller but significant differences in deviance reduction, 0.1-10 %, but their contribution to the accuracy of category prediction is highly limited by themselves.

Table 9 also shows the estimated odds of the parameters. A negative shift of $\mathrm{U_{h_2}}$ increases the odds for η_2 and η_3. It corresponds to shifting the inactivation of $\mathrm{Na_{TTX-R}}$ towards depolarized potentials, releasing the system from inactivation. The response effects of the other parameters appear tuned to the same mechanism. Positive values of $\mathrm{U_{n_1}}$, the activation

Parameter	**dev**	**% red**	**exp(β_3)**	**% ac$_3$**	**exp(β_2)**	**% ac$_2$**
$\overline{g}_{Na_{TTX-R}}$	13.1	0.2	1.14	0	1.02	0
U_{m_1}	24.7	0.3	1.14	0	0.86	0
U_{m_2}	139.6	1.8	1.07	0	1.88	0
U_{h_2}	2207.4	28.4	0.10	55.8	0.14	0
k_{m_2}	10.4	0.1	0.91	0	1.08	0
U_{n_1}	208.8	2.7	1.59	0.9	1.60	0
U_{q_1}	50.6	0.7	1.29	0	1.08	0
U_{q_2}	27.7	0.4	1.20	0	1.04	0
k_{h_3}	10.9	0.1	0.89	0	0.95	0
V_i	85.9	1.1	0.76	0	0.72	0
S	580.2	7.2	0.41	14.1	1.23	0

Table 9: Response effects of parameter variation one at the time (OAT). "dev" denotes the deviance of the multinomial logistic regression model with a single parameter compared to the intercept-only model. "red" denotes the reduction of deviance in percentage compared to the intercept-only model. "exp(β_2)" and "exp(β_3)" refer to estimated linear effects of parameter variation on odds for response cluster 2 and 3 respectively. The increase in classification accuracy for cluster 2 and 3 is reported under "% ac$_2$" and "% ac$_3$" respectively.

midpoint of the delayed potassium current, increase the odds for η_2 and η_3. This involves shifting the activation curve towards hyperpolarized potentials, which ought to release the system from inactivation, thereby favoring firing responses. Also the impact of the H-currents is in line with this, although the effects are weak. U_{q_1} and U_{q_2} raise the firing odds when shifted in the positive direction, i.e. when reducing the Q conductance, which hyperpolarizes and makes the membrane more negative.

The effect of S is more equivocal than the effects other parameters. A negative S raises the odds for η_3, but a positive S favors the odds for η_2. In the default Herzog model, negative stimuli do in fact generate stronger responses than positive ones. The explanation is that negative stimuli release the system from a state of inactivation, whereas positive stimuli favor it. However, the effect is non-systematic. There is no steady change of output in response to steady change of input.

Because of the dominance of U_{h_2}, we make it an obligatory regressor/predictor when elaborating the logistic model and incorporating multiple regressors/predictors. We add the remaining 31 parameters, as well as all pair-wise interaction terms between them ($P_i * P_j, i, j \in 1...32, i \neq j$), OAT to a logistic model that always includes U_{h_2}. We check for larger deviance effects. This analysis confirms the importance of the parameters in table 9, as well as some others with very low deviance (< 10). To select

Parameter	β_2	**SE**	**Wald**	**df**	**p**	**exp(β_2)**	**% ac$_2$**
Intercept	-3.15	0.10	950.57	1	0.00		
U_{h_2}	-2.83	0.12	560.61	1	0.00	0.06	19.1
S	-0.43	0.08	31.67	1	0.00	0.65	17.9
U_{n_1}	0.95	0.08	151.21	1	0.00	2.58	7.0
V_i	-0.70	0.07	105.18	1	0.00	0.50	5.5
U_{m_2}	0.76	0.07	122.82	1	0.00	2.15	10.1
U_{q_1}	0.25	0.07	15.15	1	0.00	1.29	2.6
$U_{m_2} * V_{n_1}$	0.56	0.07	58.82	1	0.00	1.76	5.3

Table 10: Final estimates for weak responses from multinomial logistic regression of η_2 on system parameters. β_2 refers to the log odds coefficients for weak responses, with the standard error given under "SE". The "Wald" statistic is used to test the significance "p" of the coefficients, assuming the Chi-square distribution with "df" degrees of freedom. The column "ac$_2$" gives the decrease in classification accuracy of weak responses without the parameter, keeping the remaining parameters in the regression model.

model parameters for further analysis, we apply a classification criterion, i.e. parameter contributions to classification accuracy. We include only parameters that increase prediction accuracy for either η_2 or η_3 by 1%. This adds six parameters and one interaction term to the final logistic model: U_{m_2}, U_{h_2}, U_{n_1}, U_{q_1}, V_i, S, and U_{m_2}*U_{n_1}. The model has a total predication accuracy of 86.1 %: 81.5 % for η_3, 20.8 % for η_2, and 95.1 % for η_1, with pseudo R-Square is 52.8 % (McFadden).

Tables 10 and 11 present estimates of the final logistic regression of η on model parameters. The importance of U_{h_2} is reinforced in the final model. In the initial analysis OAT, one standard unit of U_{h_2} in the negative direction increases the odds for η_3 by 7.1 (0.14 in the positive direction). In the final model, the corresponding value is 50 (0.02). The impact of U_{n_1} also increases. Furthermore, U_{m_2} reinforces its dampening function, favoring η_2 over η_3. The effect of U_{q_1} remains weak and the impact of S changes character. It looses its counter-effects on η_2 and η_3, retaining its odds function for η_3, but reverses for η_2.

4.2 Modulators of firing frequency

The distribution of frequency responses ω for η_3 is close to normal (figure 5). For optimal fit, i.e. maximal correlation between ordered sample values $\omega*$ and corresponding quantiles of the standard normal distribution (4.5), we apply power transformation. A transformation with k=0.6280 results in maximal correlation of 0.9993 for n=1046 cases.

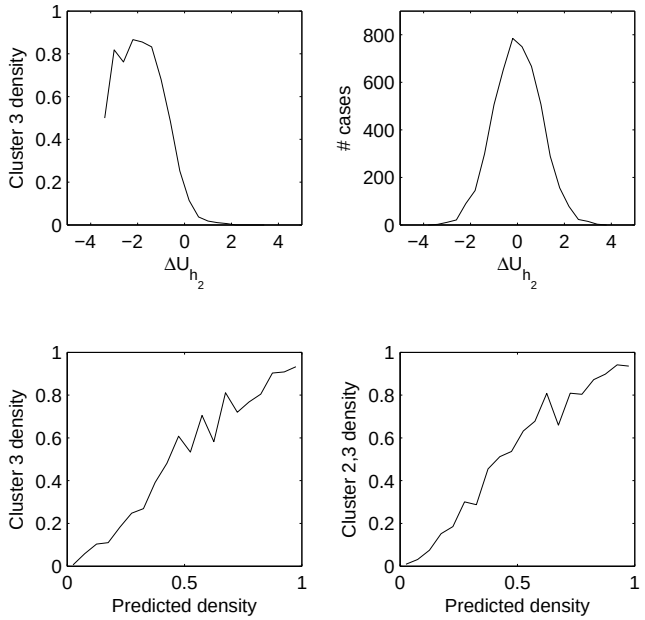

Figure 4: Illustrations of logistic regression. The upper left plot renders the density of η_3 with respect to $\mathrm{U}_{\mathrm{h}_2}$, showing the support for a logistic predictive function. It appears to reverse direction at highly negative potentials, but the limited number of observations at these potentials makes any conclusion uncertain. The upper right plot shows the normal density of $\mathrm{U}_{\mathrm{h}_2}$. The lower plots represent the density of η_2 and η_3 with respect to predicted response class ($\hat{\eta_2}$ and $\hat{\eta_3}$), confirming approximately linear relationships.

Parameter	β_3	**SE**	**Wald**	**df**	**p**	**exp(β_3)**	**% ac$_3$**
Intercept	-3.44	0.11	929.12	1	0.00		
U_{h_2}	-3.88	0.13	938.89	1	0.00	0.02	55.5
S	-2.00	0.08	571.86	1	0.00	0.14	12.1
U_{n_1}	1.32	0.07	342.77	1	0.00	3.74	7.0
V_i	-0.86	0.06	175.28	1	0.00	0.42	3.3
U_{m_2}	0.11	0.06	3.30	1	0.05	1.12	2.2
U_{q_1}	0.55	0.06	80.14	1	0.00	1.73	2.0
$U_{m_2} * U_{n_1}$	0.74	0.07	126.21	1	0.00	2.10	3.3

Table 11: Final estimates for firing responses from multinomial logistic regression of η_3 on system parameters. β_3 refers to the log odds coefficients for weak responses, with the standard error given under "SE". The "Wald" statistic is used to test the significance "p" of the coefficients, assuming the Chi-square distribution with "df" degrees of freedom. The column "ac$_3$" gives the decrease in classification accuracy of proper firing responses without the parameter, keeping the remaining parameters in the regression model.

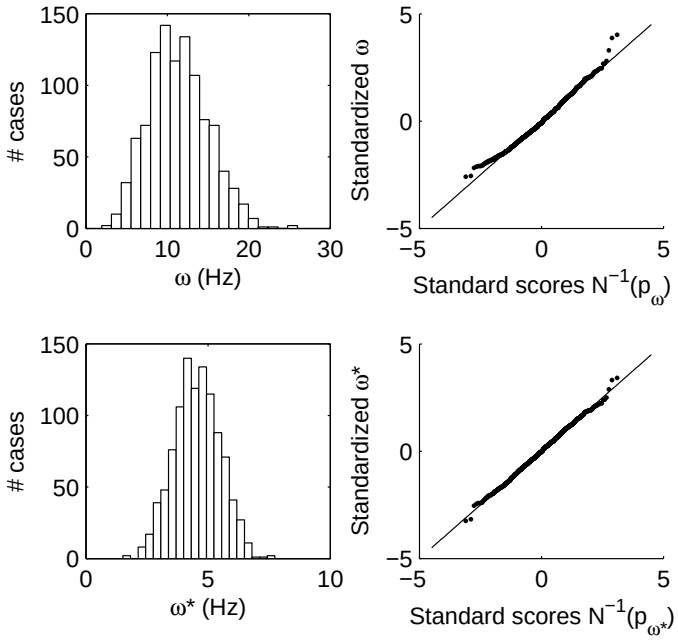

Figure 5: The distribution of frequency responses, before ω and after $\omega*$ power transformation.

Parameter	**B**	**SE**	**t**	**p**
Intercept	3.804	0.040	93.973	0.000
U_{h_2}	-0.756	0.027	-27.641	0.000
k_{m_2}	0.381	0.023	16.690	0.000
V_i	-0.380	0.019	-20.184	0.000
U_{m_2}	0.331	0.017	19.525	0.000
S	0.140	0.021	6.665	0.000
U_{n_1}	0.160	0.018	8.927	0.000

Table 12: Linear regression estimates of parameter effects on dominant frequency ω*.

$$\omega* = \omega^k, k \in \left\{ R : max\left(corr\left(\omega_i^k, N^{-1}\left(\frac{i}{n+1} \right) \right) \right) \right\} \qquad (4.5)$$
$$i \in \{1, ..., n : \omega_1 < ... < \omega_n\}$$

Linear regression of $\omega*$ on standardized values of 32 parameters OAT reveals eleven significant parameters. U_{h_2} is the parameter with the largest coefficient of determination (R^2=0.25), i.e. the parameter that accounts for the largest proportion of the response variation, but its dominance is not as pronounced as in the logistic case. When elaborating a linear model with U_{h_2}, adding other parameters and interaction terms OAT, stepwise, we get model with six parameters, and without interaction terms: R^2=0.665 (F(6,1039)=344.2, p<0.001).

U_{h_2} remains the most significant parameter (table 14). Negative values increase frequency. Thus, U_{h_2} is both a regulator of firing behavior and a modulator of firing frequency. This is also the case for U_{n_1} and U_{m_2}, positive values favoring firing odds and higher frequency. However, the effect of U_{m_2} is not too clear. In the logistic case, it raises the odds for η_2, weak responses, rather than η_3. This indicates that the effect of U_{m_2} is irregular rather than supporting a response function. The parameter k_{m_2}, the slope (the voltage sensitivity) of the activation function of Na_{TTX-R}, had no effect at all in the logistic model, but has a clear effect on $\omega*$. A larger slope implies a reduction in the voltage sensitivity and a higher frequency response.

The effect of V_i is systematic. Higher positive values increase the odds for $\eta_{2,3}$ and raise the frequency $\omega*$. This is consistent with a release function, i.e. releasing the system from inactivation by negative shifts of voltage potentials. However, the parameter is not interesting in itself. The initial membrane potential lacks distinct physiological correlates. At most, it corresponds to the sum of all previous neuronal activity and stimuli, defining the membrane potential at a given time. It hardly makes a reliable regulator or modulator of neuronal activity. In this study, we included V_i only to randomize system conditions.

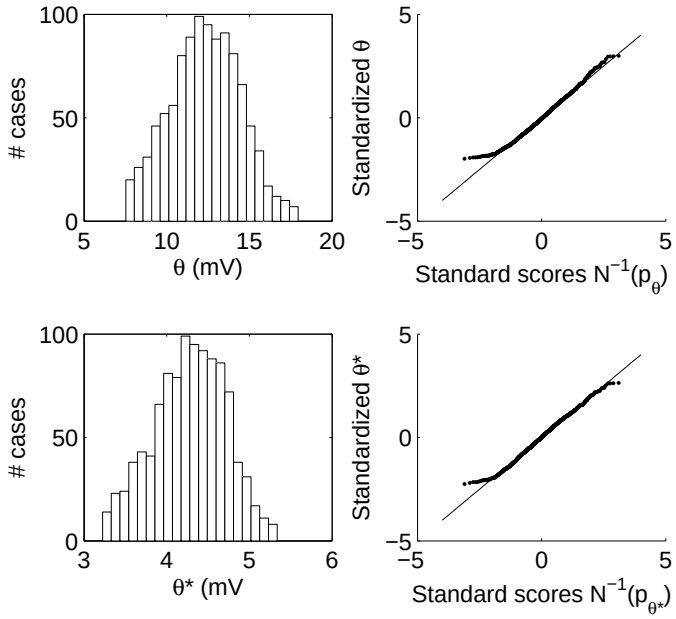

Figure 6: The distribution of dominant amplitude before θ and after $\theta*$ power transformation.

In the logistic model, there is a negative correlation between S and firing odds, negative S favoring firing odds, although the effects were not altogether clear and consistent. In the linear model, the correlation between S and $\omega*$ is positive, positive S raising the frequency. This confirms the non-systematic impact of S and the need for alternative mechanisms of firing.

4.3 Modulators of firing amplitude

The distribution of dominant amplitude θ for η_3 is close to normal (figure 6). The fit is optimized by power transformation. Applying the criterion of maximal correlation between transformed sample values $\theta*$ and their corresponding quantiles results in a correlation of 0.9976 for k=0.58 and n=1046 cases.

To identify modulators of amplitude, we apply linear regression of model parameters on dominant amplitude $\theta*$. The analysis is carried out in the same step-wise manner as in previous cases, beginning with parameters OAT, and then adding them one after another. The result is a less clear-cut set of parameters. About 20 parameters demonstrate significant effects. By limiting the analysis to the ones that contribute to R^2 more than 2.5%, we are left with a final model with six parameters (R^2=0.753, F(6,1039)=527.4,

Parameter	**B**	**SE**	**t**	**p**
Intercept	11.852	0.076	156.944	0.000
U_{m_1}	0.520	0.032	16.254	0.000
U_{h_1}	-1.130	0.034	-33.454	0.000
U_{m_2}	-1.126	0.044	-25.408	0.000
U_{h_2}	0.651	0.051	12.724	0.000
U_{n_1}	0.543	0.035	15.425	0.000
S	-1.316	0.041	-32.030	0.000

Table 13: Linear regression estimates of parameter effects on dominant amplitude $\theta*$.

$p<0.001$).

The analysis reveals a moderate reversed modulatory role of the TTX-resistant Na^+-conductance for response effects. Shifts of voltage midpoints of activation and inactivation U_{m_2} and U_{h_2} that favor firing responses $\eta_{2,3}$ and $\omega*$ reduce amplitude $\theta*$. The effect is weak, but it indicates a limit to the regulatory role of U_{h_2}. Too strong negative shifts may be counterproductive for firing dynamics. Also S demonstrates inconsistent effects on firing behavior. Negative values of S reduce $\omega*$, but increase $\theta*$. U_{n_1} is the only consistent model parameter, favoring firing response on all response measures when shifted in the hyperpolarized direction, even if the effect is relatively weak compared to U_{h_2} and S.

The linear regression on $\theta*$ also reveals two new parameters to firing dynamics: the voltage midpoints of activation and inactivation (U_{m_1} and U_{h_1}) of the TTX-sensitive Na^+-conductance (Na_{TTX-S}). Amplitude increases with negative and positive shifts of U_{m_1} and U_{h_1} respectively.This is in agreement with previous experimental and modeling studies, showing that Na_{TTX-S} modulates the amplitude of spikes, rather than generating spikes.

5 From statistics to mechanics

The statistical sensitivity analysis confirms response effects of a limited number of parameters. They indicate alternative pathways of firing than stimulus-response. However, the analysis is based on an unrealistic assumption, i.e. normal parameter distributions. In real neurons, the variation of the physiological correlates to model parameters are far from smooth, monotone and regular. For example, voltage midpoints of activation and inactivation are shifted in discrete steps due to a variety of biochemical interactions. To make credible hypotheses and predictions, we need to translate our statistical findings into realistic model components.

Considering the large number of model parameters, the analysis needs

to be limited. The statistical sensitivity analysis revealed the importance of four parameters for all three response measures: the midpoint of inactivation of Na_{TTX-R} (U_{h_2}), the midpoint of activation of K (U_{n_1}), stimulus (S) and the initial membrane potential (V_i). S and V_i are here dropped from the discussion. They are functions of many transduction and conductance processes and do not correspond to any distinct conductance mechanism. We are left with U_{h_2} and U_{n_1}, but add two parameters, U_{m_2}, the midpoint of activation of Na_{TTX-R}, and k_{m_2}, the slope of activation of Na_{TTX-R}. The roles of U_{m_2} and k_{m_2} are not prominent, but interesting. They are components of the same conductance as U_{h_2} and appear to have opposite effects on firing responses, disrupting and supporting responses respectively.

5.1 From graded effects to discrete conductance shifts

As mentioned in the introduction, the physiological correlates to parameter variation are of different kinds: (1) between cell variation, phenotypic traits, e.g. morphology, (2) within cell variation, electro- and biochemical regulation, e.g. transduction processes (3) physical fluctuations (random variation). All three sources of variation manifest themselves in shifts of the activation and inactivation midpoints of ion channels and receptors. The largest variation exists between neurons and neuronal populations. The smallest arises from physical fluctuations. Our focus here is on activation and inactivation shifts due to electro- and biochemical regulation, i.e. shifts in the order of 5-50 mV.

The logistic regression analysis shows that negative shifts of U_{h_2} increases the odds for firing. According to this statistical model, the shift may take any value. This is not a realistic assumption. First, there are lower and upper limits to the magnitude of a shift serving regulatory processes, 5-50 mV. Second, a shift is discrete in nature, not graded. It arises due to specific molecular interactions causing an all-or-none change. Thus, we need translate this graded shift into a discrete one.

We begin by calculating the effect of a discrete shift of the inactivation midpoint of Na_{TTX-R}, U_{h_2}. Given the logistic regression analysis, shifting it by two standard units in the negative direction, i.e. ≈ -10 mV, increases the odds for firing against non-firing from 3:100 to about 75:1. Two standard units account for 95% of the observations in the sample. Beyond that, we cannot be sure of the effects. Therefore we let two standard units be an upper limit to all activation and inactivation shifts, including U_{m_2} and U_{n_1}.

To remodel the activation and inactivation shifts, we define new conductance components in the original model. For each midpoint shift, we duplicate the original current/conductance (I_{shift}) and edit the activation or inactivation midpoint of the gating function in question, for example h_{2s}, which stands for a shifted gating inactivation function of the Na_{TTX-R} conductance. The new conductances are similar to their originals except for

the shifted midpoints. We hypothesize discrete shifts in the order of 10 mV, in the negative direction for U_{h_2}; in the positive direction for U_{m_2} and U_{n_1}. The following equations illustrates the shifted Na_{TTX-R} conductance:

$$I_{Na_{shift}} = \zeta * \overline{g}_{Na_{TTX-R}} m_2 h_{S2} (V - E_{Na}) \tag{5.1}$$

$$\frac{dh_{2s}}{dt} = \frac{h_{2s}(\infty) - h_{2s}}{\tau_{h_{S2}}} \tag{5.2}$$

$$h_{2s}(\infty) = \frac{\alpha_{h_{2s}}}{\alpha_{h_{S2}} + \beta_{h_{S2}}}$$

$$\tau_{h_{S2}} = \frac{2}{\alpha_{h_{2s}} + \beta_{h_{2s}}}$$

$$\alpha_{h_{2s}} = \frac{0.06435}{1 + e^{\frac{V+73.26415-10}{3.71928}}} \tag{5.3}$$

$$\beta_{h_{2s}} = \frac{0.13496}{1 + e^{\frac{V+10.27853-10}{-9.09334}}} \tag{5.4}$$

For the sake of simplicity, the shift of k_{m_2}, the slope of activation, is treated in a similar manner as midpoints of activation and inactivation. A shift is in the order of 2 standard units in the direction that favors response changes. It could be argued that slopes of activation and inactivation (voltage sensitivity) are graded in kind, depending on ionic gradients, rather than discrete due to single molecular interactions. However, for the sake of demonstrating the method of remodeling, we here simply assume that slope shifts are discrete.

We keep the total density of the conductances constant, but varies the proportion of shifted and non-shifted conductances ($\zeta \in [0,1]$). The physiological correlate of this would be a change in concentration of non-shifted and shifted Na_{TTX-R}-conductances (ion channels). Thus, this remodeling of shifts of midpoints makes for more realistic modeling, discrete rather than graded shifts, while still allowing for graded modulation at the level of maximal conductances. In the next section, we present the results of simulations that include the shifted conductance components.

5.2 Dual firing mechanisms

To explore the effects of remodeling, we run simulations with shifted U_{h_2}, U_{m_2} and U_{n_1}, and with default values of the remaining model parameters. We use the same simulation protocol and response measures as in the random sampling: Matlab ODE45, 1 second response time and 1 μs time steps. Here we limit the discussion to the frequency responses with respect to δ, the proportion of shifted conductance. We use nine different remodeling conditions "SC-X" (Shifted Conductance Case No X).

Shifted Conductance	**Description**
SC-1	Shifting U_{h_2} -10 mV
SC-2	Shifting U_{n_1} +10 mV
SC-3	Shifting U_{h_2} -10 mV and U_{n_1} +10 mV
SC-4	Shifting U_{h_2} -10 mV and U_{m_2} +10 mV
SC-5	Shifting U_{n_1} +10 mV and U_{m_2} +10 mV
SC-6	Shifting U_{h_2} -10 mV, U_{n_1} +10 mV and U_{m_2} +10 mV
SC-7	Shifting U_{h_2} -10 mV and k_{m_2} + 2 standard units (s.u.)
SC-8	Shifting U_{n_1} -10 mV and k_{m_2} + 2 s.u.
SC-9	Shifting U_{h_2} -10 mV, U_{n_1} -10 mV and k_{m_2} + 2 s.u.

Table 14: Nine conditions for simulating frequency effects of shifted conductances of U_{h_2}, U_{m_2}, U_{n_1} and k_{m_2}.

In figure 7, we show nine plots illustrating the effects of remodeling U_{h_2}, U_{m_2} and U_{n_1}. The top left plot shows the effect of shifting U_{h_2} alone, -10 mV, all other parameters at their default values. It demonstrates a monotone response function of density. Also U_{n_1} demonstrates the capacity to induce firing responses on its own (c.f. SC-2). To test if any other model parameter can induce firing responses on their own, we applied conductance shifts to all other model parameters. Only U_{h_2} and U_{n_1} have this capacity. The effect of U_{n_1} appears weaker compared to U_{h_2}. Still, the effects of U_{n_1} and U_{h_2} are complementary. The threshold of firing is higher for U_{n_1} and its range of response frequencies lower, which agrees with the regression analysis. This indicates that it is in principle possible for different transduction pathways to act through different response, thereby enabling dual coding of stimuli.

In the third plot (SC-3), we add both shifted U_{h_2} and U_{n_1} to our model. The result is not too different from U_{h_2} alone. The frequency function raises more sharply, but otherwise no major difference. In plots 3-6, we check the effects of discrete shifts of U_{m_2}; first when added to a model with shifted U_{h_2} (SC-4); then together with shifted U_{n_1} (SC-5); and last all three together (SC-6). The pattern is inconsistent, which agrees with our regression analysis. U_{m_2} both increases and decreases firing responses. In contrast, k_{m_2} generates more consistent response patterns. When added to shifted U_{h_2} model (SC-7), it broadens the range of response frequencies, but does not change the threshold. It has less of an effect together with U_{n_1} (SC-8). Adding U_{h_2}, U_{m_2} and k_{m_2} together (SC-9), the result is similar to U_{h_2} and k_{m_2} alone.

Overall, the remodeling of conductance components supports and refines the regression analysis. U_{h_2} and U_{n_1} have independent complementary effects, mediating the response effects of U_{m_2} and k_{m_2}. k_{m_2} appears to have a consistent modulatory role, increasing the firing frequency of U_{h_2} shifts. Considering that ion channel modulation targets single proteins, this inter-

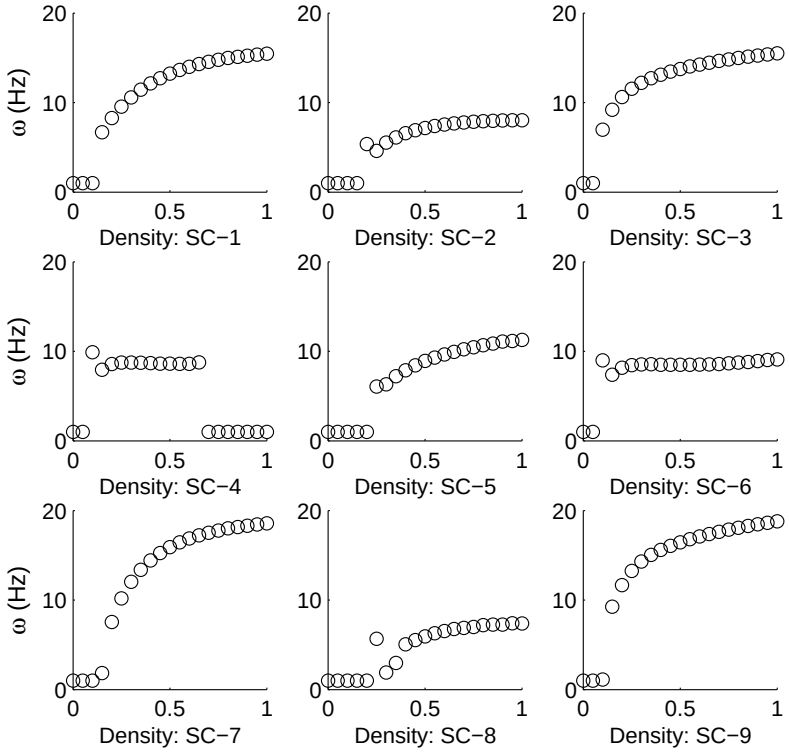

Figure 7: To evaluate response functions of parameter variations, indicated by regression analysis, we remodel conductance components by adding shifted versions to the original conductance components in the model. The conductances are the same except for shifted parameter values in agreement with the regression analysis. We keep the total density of a particular conductance constant, $\mathrm{Na}_{\mathrm{TTX-R}}$ for example, but varies the proportion of shifted and non-shifted parts ($\delta = [0, 1]$). The remaining model parameters are at their default values. We render nine plots of the remodeling effects on response frequency ω. "SC-X" stands for Shifted Conductance No X. SC-1: shifting $\mathrm{U}_{\mathrm{h}_2}$ alone, -10 mV, results in a monotone response function of density. SC-2: shifting $\mathrm{U}_{\mathrm{n}_1}$ alone, 10 mV, also demonstrates a frequency response function, but weaker in effect (firing threshold and frequency range). No other parameters have the capacity to induce firing on their own. SC-3: shifting $\mathrm{U}_{\mathrm{h}_2}$ and $\mathrm{U}_{\mathrm{n}_1}$ together indicates no larger interaction effects. SC-4: shifted $\mathrm{U}_{\mathrm{m}_2}$ added to shifted $\mathrm{U}_{\mathrm{h}_2}$ generates non-linear effects. SC-5: shifted $\mathrm{U}_{\mathrm{m}_2}$ added to shifted $\mathrm{U}_{\mathrm{n}_1}$ gives a slight increase in effects of the latter. SC-6: shifted $\mathrm{U}_{\mathrm{m}_2}$ added to both shifted $\mathrm{U}_{\mathrm{h}_2}$ and shifted $\mathrm{U}_{\mathrm{n}_1}$ has a dampening effect. SC-7: shifted $\mathrm{k}_{\mathrm{m}_2}$ added to shifted $\mathrm{U}_{\mathrm{h}_2}$ increases the frequency range of the response function. SC-8: shifted $\mathrm{k}_{\mathrm{m}_2}$ added to shifted $\mathrm{U}_{\mathrm{n}_1}$ has limited effects. SC-9: shifted $\mathrm{k}_{\mathrm{m}_2}$ added to both shifted $\mathrm{U}_{\mathrm{h}_2}$ and shifted $\mathrm{U}_{\mathrm{n}_1}$ has effects similar to $\mathrm{k}_{\mathrm{m}_2}$ and $\mathrm{U}_{\mathrm{h}_2}$ alone.

action is reasonable. It is more reasonable with joint shifted activation and inactivation for one and the same conductance, U_{h_2} and k_{m_2}, rather than for different conductances, U_{n_1} and k_{m_2}.

6 Discussion

Depending on purpose, we describe and explain firing dynamics of single neurons with models at different levels of abstraction. On the one hand, experimentalists tend to define detailed models on the basis of particular experiments and neurons (Hodgkin and Huxley 1952). The purpose is to synthesize and summarize research findings. On the other hand, mathematicians formalize abstract models. The purpose is then to define the most general properties of system dynamics (Izhikevich 2007). Without any doubt, both approaches are important for developing and testing theories of system dynamics of single neurons. We need to know both general and specific properties of firing dynamics. However, to strengthen the predictive power of our models, we must also connect the different levels of abstraction. In this article, we applied statistical sensitivity analysis and system remodeling to this end.

When modeling neuronal excitability with Hodgkin-Huxley-like models, we tend to keep parameters constant for the purpose of describing firing mechanisms. In this study, we have shown that statistical sensitivity analysis of parameter variations can be used to reveal other mechanisms of firing dynamics than the traditional one: stimulus-response. By varying midpoints and slopes of activation and inactivation, as well as conductance densities, we have identified ion channel components that can regulate neuronal excitability and themselves be targets of transduction pathways and processes, i.e. biochemical regulation by means of molecular interactions.

The analysis indicates that the inactivation midpoint of the Na_{TTX-R}-current plays a critical role. Shifting it induces firing and generates linear frequency responses. In experimental studies, the inactivation part of the ion channel does in fact generate disturbances of the neuronal excitability (Cummins et al 2007; Rush et al 2006). The same goes for the activation midpoint of the delayed potassium rectifier. Also this conductance has been implicated in excitability disturbances in experimental studies (Sun et al 2006). Their effects may be induced independent of each other, which opens up the possibility for complementary transduction pathways to the excitability of nociceptors. The activation of different receptors, mechano- and thermosensitive receptors for example, may target the inactivation of Na_{TTX-R} and the activation of K_{dr} respectively. Thus, these sensory neurons are not only relaying stimuli, but actually interpreting them.

These conclusions are but hypotheses that need to be expanded and elaborated by both experimental and modeling studies. We believe that

statistical sensitivity analysis has an important role to play here. Traditionally, research on membrane excitability ends up specifying response functions (gain functions) describing how response frequency changes as a function of stimulus intensity. The purpose is usually a descriptive summary of observable relations between input and output. It is rarely possible to study more than a few variables and variations of experimental conditions. In contrast, the number of parameters is not really the problem in modeling studies, but making good and relevant predictions. Here statistical sensitivity analysis serves its purpose. It adds generality to experimental models and predictive value to modeling studies.

A fundamental assumption here is that the explanatory value and predictive power of a model is intrinsically linked to some methods of observation and measurement. To the extent that a model disregards conditions of observation, or adds spurious ones, it looses value and power. For this reason, we choose to stay close to the classic Hodgkin-Huxley approach, whole-cell measurements, which is still a very important method in experimental neurophysiology. However, to analyze nociceptors and verify their firing mechanisms in detail, we need to extend the approach. In particular, when dealing with polymodal nociceptors, we need to integrate experimental models of both transduction and conduction processes. Considering the complexity of this parameter space, statistical sensitivity analysis may then become of even greater value and use.

7 Acknowledgements

This work is supported by Swedish Foundation for Strategic Research and The Foundation of Helge Ax:son Johnson.

References

[1] Amir R, Michaelis M, Devor M. (1999). Membrane potential oscillations in dorsal root ganglion neurons: role in normal electrogenesis and neuropathic pain. The Journal of Neuroscience. 19(19):8589-96.

[2] Cavanaugh DJ, Lee H, Lo L, Shields SD, Zylka MJ, Basbaum AI, Anderson DJ. (2009). Distinct subsets of unmyelinated primary sensory fibers mediate behavioral responses to noxious thermal and mechanical stimuli. Proceedings of the National Academy of Sciences of the United States of America. 106(22):9075-80.

[3] Cummins TR, Sheets PL, Waxman SG. (2007) The roles of sodium channels in nociception: Implications for mechanisms of pain. Pain. 131(3):243-57.

[4] Davison, A.C. (2003). Statistical models. Cambridge, US: Cambridge University Press.

[5] Devor M. (1999). Unexplained peculiarities of the dorsal root ganglion. Pain. Aug;Suppl 6:S27-35.

[6] Dobson A, Barnett A.G. (2008). An Introduction to Generalized Linear Models. Third Edition. Boca Raton, US: CRC Press.

[7] Everill B, Rizzo MA, Kocsis JD. (1998). Morphologically identified cutaneous afferent DRG neurons express three different potassium currents in varying proportions. Journal of Neurophysiology. 79(4):1814-24.

[8] Herzog RI, Cummins TR, Waxman SG. (2001). Persistent TTX-resistant Na+ current affects resting potential and response to depolarization in simulated spinal sensory neurons. Journal of Neurophysiology. 86(3):1351-64.

[9] Hodgkin, A.L. and Huxley, A.F. (1952). A quantitative description of membrane current and its application to conduction and excitation in nerve. The Journal of Physiology. 117:500-544.

[10] Ingalls B. (2008). Sensitivity analysis: from model parameters to system behaviour. Essays in Biochemistry. 45:177-93.

[11] Izhikevich, E.M. (2007). Dynamical systems in neuroscience: The geometry of excitability and bursting (författare) Cambridge, Massachusetts: MIT Press.

[12] Johnson R.A. and Wichern D.W. (2007). Applied Multivariate Statistical Analysis. Upper Saddle River, US: Prentice Hall. 6th Ed.

[13] Koch, C. (1999). Biophysics of computation : information processing in single neurons. New York, US.: Oxford University Press.

[14] Kouranova EV, Strassle BW, Ring RH, Bowlby MR, Vasilyev DV. (2008). Hyperpolarization-activated cyclic nucleotide-gated channel mRNA and protein expression in large versus small diameter dorsal root ganglion neurons: correlation with hyperpolarization-activated current gating. Neuroscience. 153(4):1008-19.

[15] Marino, S., Hogue, I.B., Ray, C.J., and Kirschner, D.E. (2008). "A methodology for performing global uncertainty and sensitivity analysis in systems biology". In Journal of Theoretical Biology. 254:178-196.

[16] Matsutomi T, Nakamoto C, Zheng T, Kakimura J, Ogata N. (2006). Multiple types of Na(+) currents mediate action potential electrogenesis in small neurons of mouse dorsal root ganglia. Pflugers Arch. 453(1):83-96.

[17] Momin A, Cadiou H, Mason A, McNaughton PA. (2008). Role of the hyperpolarization-activated current Ih in somatosensory neurons. The Journal of Physiology. 586(24):5911-29.

[18] Okuse K. (2007). Pain signalling pathways: from cytokines to ion channels. International Journal Biochemistry & Cell Biology. 39(3):490-6.

[19] Olausson B. (1998). Recordings of polymodal single c-fiber nociceptive afferents following mechanical and argon-laser heat stimulation of human skin. Experimental Brain Research. 122(1):44-54.

[20] Prescott SA, De Koninck Y, Sejnowski TJ. (2008). Biophysical basis for three distinct dynamical mechanisms of action potential initiation. PLoS Computational Biology. 4(10):e1000198.

[21] Rieke, F., Warland, D., van Steveninck, R.R., and Bialek, W. (1999). Spikes: Exploring the Neural Code. Cambridge, Massachusetts U.S.: MIT Press.

[22] Rush AM, Cummins TR, Waxman SG. (2007). Multiple sodium channels and their roles in electrogenesis within dorsal root ganglion neurons. Journal of Physiology 579(1):1-14.

[23] Rush AM, Dib-Hajj SD, Liu S, Cummins TR, Black JA, Waxman SG. (2006). A single sodium channel mutation produces hyper- or hypoexcitability in different types of neurons. Proc Natl Acad Sci USA vol. 103 (21) pp. 8245-50

[24] Saltelli, A., Chan, K., and Scott, E.M. (Eds.) (2000). Sensitivity Analysis. Chichester, UK: John Wiley & Sons Ltd.

[25] Schild JH, Clark JW, Hay M, Mendelowitz D, Andresen MC, Kunze DL. (1997). A- and C-type rat nodose sensory neurons: model interpretations of dynamic discharge characteristics. Journal of Neurophysiology. 78(6):3198-209.

[26] Schmelz M., Schmidt R. (2009). Microneurographic single-unit recordings to assess receptive properties of afferent human C-fibers. Neuroscience Letters. May 28.

[27] Smith ES, Lewin GR. (2009). Nociceptors: a phylogenetic view. Journal of Comparative Physiology: A Neuroethology, sensory, neural, and behavioral physiology.

[28] Stelling J, Gilles ED, Doyle FJ 3rd (2004). Robustness properties of circadian clock architectures.Proc Natl Acad Sci U S A. 101(36):13210-5.

[29] Sun JH, Yang B, Donnelly DF, Ma C, LaMotte RH. (2006). MCP-1 enhances excitability of nociceptive neurons in chronically compressed dorsal root ganglia. The Journal of Neurophysiology. 96(5):2189-99.

[30] Belmonte, C. and Viana, F. (2009). Nociceptor Responses. Encyclopedia of Neuroscience. 6:1191-1198.

[31] Waxman. (2006). Neurobiology: a channel sets the gain on pain. Nature. 444(7121):831-2.

[32] Weaver CM, Wearne SL. (2008). Neuronal Firing Sensitivity to Morphologic and Active Membrane Parameters. PLoS Comput Biol 4(1): e11. doi:10.1371/journal.pcbi.0040011.